# $\alpha$-OCC: Uncertainty-Aware Camera-based 3D Semantic Occupancy Prediction

**Anonymous authors**
**Paper under double-blind review**

## Abstract

Comprehending 3D scenes is paramount for tasks such as planning and mapping for autonomous vehicles and robotics. Camera-based 3D Semantic Occupancy Prediction (OCC) aims to infer scene geometry and semantics from limited observations. While it has gained popularity due to affordability and rich visual cues, existing methods often neglect the inherent uncertainty in models. To address this, we propose an uncertainty-aware OCC method ($\alpha$-OCC). We first introduce Depth-UP, an uncertainty propagation framework that improves geometry completion by up to 11.58% and semantic segmentation by up to 12.95% across various OCC models. For uncertainty quantification (UQ), we propose the hierarchical conformal prediction (HCP) method, effectively handling the high-level class imbalance in OCC datasets. On the geometry level, the novel KL-based score function significantly improves the occupied recall (45%) of safety-critical classes with minimal performance overhead (3.4% reduction). On UQ, our HCP achieves smaller prediction set sizes while maintaining the defined coverage guarantee. Compared with baselines, it reduces up to 90% set size, with 18% further reduction when integrated with Depth-UP. Our contributions advance OCC accuracy and robustness, marking a noteworthy step forward in autonomous perception systems.

## 1 Introduction

Achieving a comprehensive understanding of 3D scenes is crucial for downstream tasks such as planning in autonomous vehicles (AVs) and robotics (Wang & Huang (2021)). 3D Semantic Occupancy Prediction (OCC) emerges as a solution that jointly infers the geometry completion and semantic segmentation (Song et al. (2017); Hu et al. (2023)). OCC approaches typically are categorized based on the sensor input: LiDAR-based OCC and camera-based OCC. While LiDAR offers precise depth information (Roldao et al. (2020); Cheng et al. (2021)), they are costly and less portable. Conversely, camera-based OCCs, with their affordability and ability to capture rich visual cues, have gained significant attention (Cao & De Charette (2022); Tian et al. (2024)). For them, depth estimation is essential for the accurate 3D reconstruction of scenes. However, existing methods frequently overlook real-world depth estimation errors (Poggi et al. (2020)). Moreover, effectively leveraging propagated depth uncertainty and rigorously quantifying OCC uncertainty, particularly in class-imbalanced datasets, remains a challenging and unexplored problem. Throughout this paper, OCC refers to camera-based OCC unless stated otherwise, which is the focus of our work.

We explain the importance of considering depth uncertainty propagation and OCC uncertainty quantification in Fig. 1. In Fig. 1(a), perturbing the ground-truth depth values by factors of $(1 + \beta)$ $(\forall\beta \in \{0\%, 2\%, 4\%, 6\%, 8\%, 10\%, 20\%\})$, simulates real-world depth estimation errors. Uncertainties of depth estimation significantly reduce the performance of OCCs. To address this, we propose a flexible uncertainty propagation framework (Depth-UP) from depth models to improve the performance of a variety of OCC models.

The OCC datasets exhibit a high class imbalance, with empty voxels comprising a significant proportion (92.91% for SemanticKITTI Behley et al. (2019)), as illustrated in the dotted box of Fig. 1(b). Bicyclist and person voxels, crucial for safety, only occupy 0.01% and 0.007% of the dataset. Consequently, networks trained on such imbalanced data, coupled with the maximum posterior classification, often overlook rare classes,

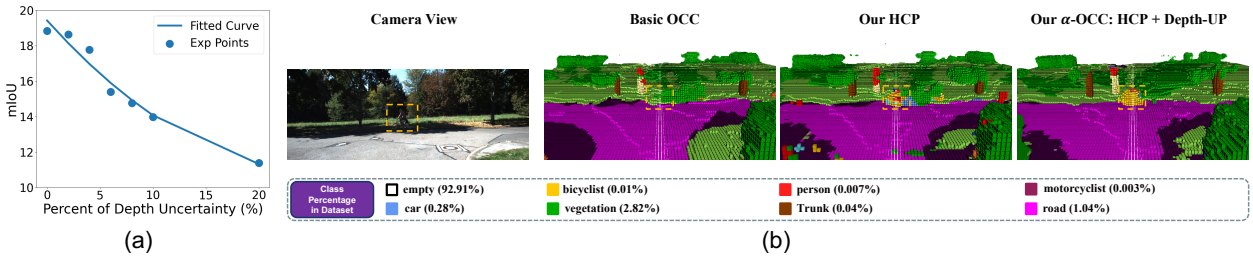


Figure 1: (a): As the percentage of depth uncertainty increases, the accuracy (mIoU↑) of OCC decreases significantly. (b): High class imbalance on OCC. The percentage next to each class is its percentage in the SemanticKITTI dataset. Since the safety-critical class "bicyclist" only occupied 0.01%, the trained OCC model fails to detect the bicyclist in front, leading to a crash. However, after quantifying the uncertainty and post-processing using our HCP, the crash is avoided, for our HCP improves the occupied recall of rare classes. When applying our Depth-UP and HCP together, safety is further enhanced as the bicyclist is more accurately identified. In contrast, using only HCP often assigns the highest probability to the car (blue) for many bicyclist voxels. Due to visualization limits, each occupied voxel shows the most probable nonempty class in the predicted set from HCP.

leading to reduced accuracy and recall (Tian et al. (2020)). This poses a significant risk in safety-critical applications like AVs, where detecting rare-class occupied voxels is essential for preventing collisions (Chan et al. (2019)). As in Fig. 1(b), a standard OCC model fails to detect the bicyclist due to the extreme rarity of the bicyclist class in the dataset. To address this, we propose a hierarchical conformal prediction (HCP) method that enhances occupied recall for rare classes in geometry completion while generating prediction sets with class coverage guarantees for semantic segmentation. By quantifying uncertainty (prediction set) through HCP, the OCC model successfully identifies rare bicyclist voxels, reducing the risk of collisions. Furthermore, our complete $\alpha$-OCC framework integrates both HCP and Depth-UP, further refines bicyclist detection, significantly improving safety.

Extensive experiments on three OCC models (VoxFormer Li et al. (2023b), OccFormer Zhang et al. (2023) and CGFormer Yu et al. (2024)) and two datasets (SemanticKITTI Behley et al. (2019) and KITTI360 Li et al. (2023a)) show that our Depth-UP improves geometry completion by 11.58% and semantic segmentation by 12.95%. Our HCP enhances person-class geometry prediction by 45% with only 3.4% IoU overhead, improving prediction on rare safety-critical classes, such as persons, thereby reducing potential risks for AVs. Compared with baselines, HCP reduces set size by 90% and coverage gap by 64%, an additional 18% set size reduction when combined with Depth-UP. These results show the significant accuracy and uncertainty quantification improvements of our $\alpha$-OCC.

Our contributions can be summarized as follows: 1) To address the challenging OCC problem, we recognize the problem from a fresh uncertainty perspective. Namely, we propose $\alpha$-OCC, an uncertainty-aware camera-based 3D semantic occupancy prediction method, which contains the uncertainty propagation (Depth-UP) from depth models to improve OCC performance and the novel hierarchical conformal prediction (HCP) method to quantify the uncertainty of OCC. 2) To the best of our knowledge, we are the first to propose the uncertainty propagation framework Depth-UP to improve OCC performance. Our approach leverages uncertainty quantified through direct modeling to improve both geometry completion and semantic segmentation, resulting in substantial performance gains across common OCC models. 3) To solve the high-level class imbalance challenge on OCC, resulting in biased prediction and low recall for rare classes, we propose the HCP. On geometry completion, a novel KL-based score function is proposed to improve the occupied recall of safety-critical classes with little performance overhead. For UQ, we achieve a smaller prediction set size under the defined class coverage guarantee. Overall, our $\alpha$-OCC shows that uncertainty is an integral and vital part of OCC tasks. Integrating Depth-UP (propagating depth uncertainty to OCC) and HCP (quantifying OCC uncertainty) enhances both accuracy and uncertainty of OCC models.

## 2 Related Work

**Uncertainty Quantification and Propagation.** Uncertainty quantification (UQ) holds paramount importance in ensuring the safety and reliability of autonomous systems such as robots (Jasour & Williams (2019)) and AVs (Meyer & Thakurdesai (2020); Su et al. (2025)). Moreover, UQ for perception can significantly enhance the planning and control processes of them (Xu et al. (2014); He et al. (2023)). Different types of UQ methods have been proposed. Monte-Carlo dropout (Miller et al. (2018)) and deep ensemble (Lakshminarayanan et al. (2017)) methods require multiple runs of inference, which makes them infeasible for real-time applications. In contrast, direct modeling (Feng et al. (2021)) estimates uncertainty in one pass, used to estimate the depth uncertainty in our work.

While uncertainty has been explored in 3D tasks, our focus differs. Eldesokey et al. (2020) improved depth completion with uncertainty by normalized convolutional neural networks. Cao et al. (2024) managed LiDAR-based OCC uncertainty with deep ensembles, increasing computational complexity. Although uncertainty propagation (UP) from depth to 3D object detection has improved accuracy (Lu et al. (2021); Wang et al. (2023)), no prior work has addressed UP from depth to OCCs. To bridge this gap, we propose Depth-UP, a direct modeling-based UP for OCCs.

Conformal prediction (CP) provides statistically guaranteed uncertainty sets for model predictions (Angelopoulos & Bates (2021); Su et al. (2024)). However, its application to class-imbalanced tasks is limited. Rare and safety-critical classes (e.g., person) remain challenging for OCC models. To address this, we propose a hierarchical conformal prediction method for uncertainty quantification in highly class-imbalanced OCCs. Related works on class imbalance are introduced in Appendix A.1. And related works on OCC are introduced in Appendix A.2.

## 3 Method

We propose $\alpha$-OCC, an uncertainty-aware OCC method integrating Depth-UP for uncertainty propagation and HCP for uncertainty quantification. Figure 2 presents the whole methodology overview and the structure of our Depth-UP. Figure 3 details our HCP. The major novelties are: *(1)* Depth-UP quantifies the uncertainty of depth estimation by direct modeling (DM) and then propagates it through probabilistic geometry projection (for geometry completion) and depth feature extraction (for semantic segmentation). *(2)* HCP calibrates OCC probability outputs. First, it predicts the voxels' occupied state by the quantile on the novel KL-based score function as Eq. 2, which can improve the occupied recall of rare safety-critical classes. Then it generates prediction sets for predicted occupied voxels, achieving a better coverage guarantee and smaller prediction set sizes.

**Preliminary:** OCC predicts a dense semantic scene within a defined volume in front of the vehicle solely from RGB images (Cao & De Charette (2022)). Specifically, with an input image $\mathbf{X} \in \mathbb{R}^{3\times H\times W}$, an OCC model first extracts 2D image features $\mathbf{F}_I$ using backbone networks like ResNet (He et al. (2016)) and estimates the depth value $\hat{\mathbf{D}} \in \mathbb{R}^{H\times W}$ for each pixel (e.g. monocular depth estimation Bhat et al. (2021) or stereo depth estimation Shamsafar et al. (2022)). Then, a probability voxel grid $\hat{\mathbf{Y}} \in [0,1]^{M\times U\times V\times D}$ is generated based on $\mathbf{F}_I$ and $\hat{\mathbf{D}}$, assigning each voxel to the class with the highest probability. Each voxel within the grid is categorized as either empty or occupied by a specific semantic class. The ground truth voxel grid is denoted as $\mathbf{Y}$, $H$ and $W$ is the height and width of the input image, $U$, $V$ and $D$ represent the height, width, and length of the voxel grid, $M$ denotes the total number of relevant classes (including the empty class), respectively.

### 3.1 Uncertainty Propagation Framework (Depth-UP)

In OCC methods, depth models facilitate the projection from 2D to 3D space, primarily focusing on geometric aspects. Nonetheless, these approaches often overlook the inherent depth uncertainty. Recognizing the potential to enhance OCC performance by utilizing this uncertainty, we introduce Depth-UP framework, which quantifies the uncertainty of depth models through a direct modeling method and propogate this uncertainty into both geometry completion and semantic segmentation to improve the final performance of various OCC models.

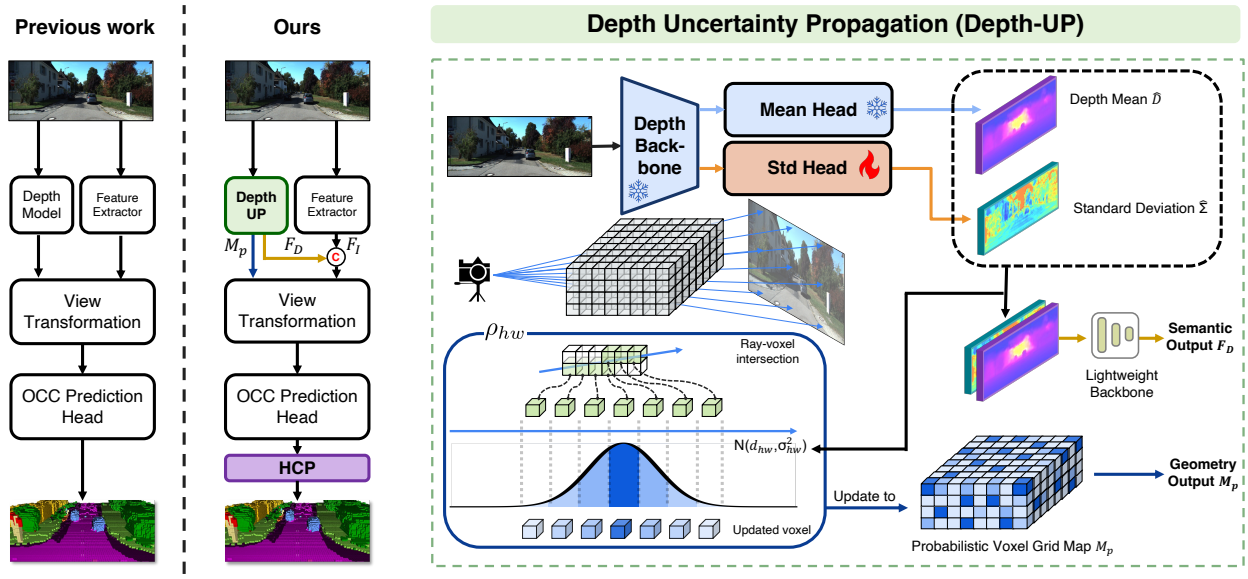


Figure 2: Overview of our $\alpha$-OCC method. The non-black colors highlight the novelties and important techniques in our method. $\mathbf{C}$ denotes the concatenation of the depth feature $\mathbf{F}_D$ and image feature $\mathbf{F}_I$. In the Depth-UP part, we calculate the uncertainty of depth estimation through direct modeling. For depth model retraining, we only train the additional standard deviation head while keeping the rest of the model frozen. Then we propagate it through depth feature extraction (for semantic segmentation) and building a probabilistic voxel grid map $M_p$ by probabilistic geometry projection (for geometry completion). Each element of $M_p$ is the occupied probability of the corresponding voxel, computed by considering the depth distribution of all rays across the voxel.

**Direct Modeling (DM).** Depth-UP includes a DM technique (Su et al. (2023); Feng et al. (2021)) to estimate the standard deviation associated with the estimated depth value of each pixel, with minimal computational overhead. An additional regression head, with a comparable structure as the original regression head for $\hat{\mathbf{D}}$, is tailored to predict the standard deviation $\hat{\mathbf{\Sigma}}$. Subsequently, this head is retrained based on the original depth model, with all parameters of the original depth model (including the original regression head) being frozen. Assume the estimated depth value is represented as a univariate Gaussian distribution, and the ground truth depth follows a Dirac delta function (Arfken et al. (2011)). For the retraining process, we define the regression loss function as the KL-divergence between the estimated distribution and the ground truth distribution, where $\mathbf{D} \in \mathbb{R}^{H \times W}$ is the ground truth depth matrix for the image: $\mathcal{L}_{KL}(\mathbf{D}, \hat{\mathbf{D}}, \hat{\mathbf{\Sigma}}) = \frac{1}{HW} \sum_{h=1}^{H} \sum_{w=1}^{W} \frac{(d_{hw} - \hat{d}_{hw})^2}{2\hat{\sigma}_{hw}^2} + \log |\hat{\sigma}_{hw}|$.

**Propagation on Geometry Completion (PGC).** Depth information is used to generate the 3D voxels on geometry in OCC. There are two key challenges: lens distortion during geometric transformations and occupied probability estimation for each voxel. Lens distortion is a deviation from the ideal image formation by a lens, resulting in a distorted image (Zhang (2000)). Existing OCC models, such as VoxFormer (Li et al. (2023b)), solve the lens distortion by projecting depth into a 3D point cloud, and then generating the binary voxel grid map $\mathbf{M}_b \in \{0, 1\}^{U \times V \times D}$, where each voxel is marked as 1 if occupied by at least one point. However, they ignore the uncertainty of depth. Here we propagate the depth uncertainty into the geometry of OCC to solve the above two challenges.

Our Depth-UP generates a **probabilistic voxel grid map** $\mathbf{M}_p \in [0, 1]^{U \times V \times D}$ that considers lens distortion and depth uncertainty, with $\{\hat{\mathbf{D}}, \hat{\mathbf{\Sigma}}\}$ from the depth model. For pixel $(h, w)$ with estimated depth mean $\hat{d}_{hw}$, we project it into point $(x, y, z)$ in 3D space: $x = \frac{(h - c_h) \times z}{f_u}, y = \frac{(w - c_w) \times z}{f_v}, z = \hat{d}_{hw}$, where $(c_u, c_v)$ is the camera center and $f_u$ and $f_v$ are the horizontal and vertical focal length.

When estimated depth follows a univariate Gaussian distribution, a point's exact location along its camera ray is uncertain. Instead, we estimate the probability of one voxel $(u, v, d)$ being occupied by points. Due

to the density of visual information, a single voxel may correspond to multiple pixels, which means a voxel can be passed by multiple rays. We denote this set of rays as $\Psi_{uvd}$, and a single ray within this set as $\rho_{hw}$, corresponding to pixel $(h, w)$. When a ray $\rho_{hw}$ passes through a voxel, it has two crosspoints: $z_s$ where the ray enters the voxel, and $z_e$ where the ray exits the voxel. By cumulating the probability of the ray inside the voxel using the probability density function, we obtain the probability of voxel $(u, v, d)$ being occupied by points:

$$\mathbf{M}_p(u, v, d) = \min\left(1, \sum_{\rho_{hw} \in \Psi_{uvd}} \int_{z_s}^{z_e} \mathcal{N}(z|\hat{d}_{hw}, \hat{\sigma}^2_{hw}) dz\right). \tag{1}$$

The original binary voxel grid map is replaced by the probabilistic voxel grid map $\mathbf{M}_p \in [0, 1]^{U \times V \times D}$ to propagate the depth uncertainty into the geometry completion of OCC.

**Propagation on Semantic Segmentation (PSS).** The extraction of 2D features $\mathbf{F}_I$ from the input image has been a cornerstone for OCC to encapsulate semantic information. However, utilizing depth uncertainty on the semantic features is ignored. Through an additional lightweight backbone, such as ResNet-18 backbone (He et al. (2016)), we extract depth features $\mathbf{F}_D$ from the concatenated depth mean and standard deviation $\{\hat{\mathbf{D}}, \hat{\mathbf{\Sigma}}\}$. These newly acquired depth features are then seamlessly integrated with the original 2D image features, constituting a novel set of input features $\{\mathbf{F}_I, \mathbf{F}_D\}$ as shown in Figure 2. This integration strategy capitalizes on the extensive insights gained from prior depth predictions, enhancing the OCC performance with enhanced semantic understanding.

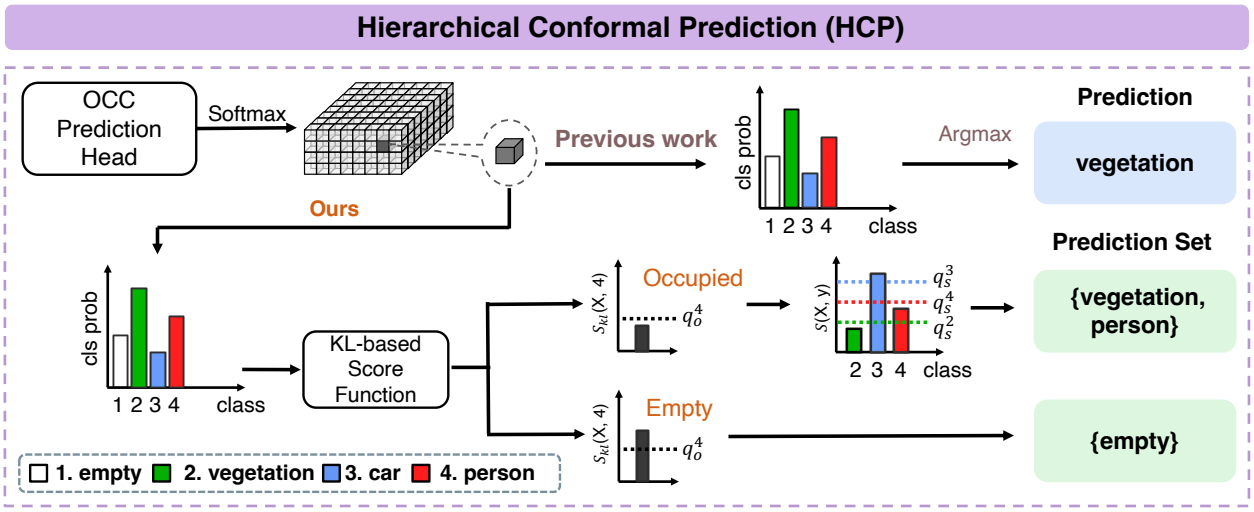


Figure 3: Overview of our Hierarchical Conformal Prediction (HCP) method. We predict voxels' occupied state by the quantile on the KL-based score as Eq. 2, which can improve occupied recall of rare classes, and then only generate prediction sets for these predicted occupied voxels. The occupied quantile $q_o^y$ and semantic quantile $q_s^y$ are computed during the calibration step of HCP.

## 3.2 Hierarchical Conformal Prediction (HCP)

### 3.2.1 Preliminary

**Standard Conformal Prediction.** For classification, conformal prediction (CP, Angelopoulos & Bates (2021); Ding et al. (2024)) is a statistical method to post-process any models by producing the set of predictions with theoretically guaranteed marginal coverage of the correct class. With $M$ classes, considering the calibration data $(\mathbf{X}_1, \mathbf{Y}_1), ..., (\mathbf{X}_N, \mathbf{Y}_N)$ with N data points that are never seen during training, the standard CP (SCP) includes the following steps: *(1)* Define the score function $s(\mathbf{X}, y) \in \mathbb{R}$ (Smaller scores indicate better agreement between $\mathbf{X}$ and $y$). The score function is a vital component of CP. A typical score function of a classifier $f$ is $s(\mathbf{X}, y) = 1 - f(\mathbf{X})_y$, where $f(\mathbf{X})_y$ represents the $y^{th}$ softmax output of $f(\mathbf{X})$. *(2)* Compute $q$ as the $\frac{\lceil (N+1)(1-\alpha) \rceil}{N}$ quantile of the calibration scores, where $\alpha \in [0, 1]$ is a user-chosen error rate.

*(3)* Use this quantile to form the prediction set $\mathcal{C}(\mathbf{X}_{test}) \subset \{1, ..., M\}$ for one new example $\mathbf{X}_{test}$ (from the same distribution of the calibration data): $\mathcal{C}(\mathbf{X}_{test}) = \{y : s(\mathbf{X}_{test}, y) \leq q\}$. The SCP provides a coverage guarantee that $\mathbb{P}(\mathbf{Y}_{test} \in \mathcal{C}(\mathbf{X}_{test})) \geq 1 - \alpha$ which has been proved in Angelopoulos & Bates (2021).

**Class-Conditional Conformal Prediction.** The SCP achieves the marginal guarantee but may neglect the coverage of some classes, especially on class-imbalanced datasets (Angelopoulos & Bates (2021)). Class-Conditional Conformal Prediction (CCCP) targets class-balanced coverage under the user-chosen class error rate $\alpha^y$, $\forall y \in \{1, ..., M\}$: $\mathbb{P}(\mathbf{Y}_{test} \in \mathcal{C}(\mathbf{X}_{test}) | \mathbf{Y}_{test} = y) \geq 1 - \alpha^y$. Every class $y$ has at least $1 - \alpha^y$ probability of being included in the prediction set when the label is $y$. Hence, the prediction sets are with coverage guarantee to all classes, even the rare ones.

### 3.2.2 Our Hierarchical Conformal Prediction

Current CP does not consider the hierarchical structure of classification, such as the geometry completion and semantic segmentation in OCCs. And it cannot achieve good coverage for very rare and safety-critical classes. Here we propose a novel hierarchical conformal prediction (HCP) to address these challenges, as shown in Figure 3. The detailed algorithm is shown in Appendix A.3.

**Geometric Level.** On the geometric level, it is important and safety-critical to guarantee the occupied recall of some sensitive classes, such as the person and bicyclist for AVs. Hence, we define the occupied coverage for the specific safety-critical class $y$ as: $\mathbb{P}(o = T | \mathbf{Y}_{test} = y) \geq 1 - \alpha_o^y$, where $o = T$ means the occupancy state is true. The probability of the voxels with label $y$ are predicted as occupied is guaranteed to be no smaller than $1 - \alpha_o^y$. The empty class is $y = 1$ and occupied classes are $y \in \{2, ..., M\}$. To achieve the above guarantee under the high class-imbalanced dataset, we propose a novel score function based on the KL divergence. Here we define the ground-truth distribution for occupancy as $\mathbf{O} = \{\varepsilon, 1, ..., 1\}^M$, where $\varepsilon$ is the minimum value for the empty class to avoid the divide-by-zero problem. With the output softmax probability $f(\mathbf{X}) = \{p_1, p_2, ..., p_M\}$ from the model $f$, we define the KL-based score function for $y \in \mathcal{Y}_r$:

$$s_{kl}(\mathbf{X}, y) = \mathrm{D}_{kl}(f(\mathbf{X}) || \mathbf{O}) = p_1 \log(\frac{p_1}{\varepsilon}) + \sum_{i=2}^{M} p_i \log(p_i), \tag{2}$$

where $\mathcal{Y}_r$ is the considered rare class set. The quantile $q_o^y$ is computed as the $\frac{\lceil (N_y+1)(1-\alpha_o^y) \rceil}{N_y}$ quantile of the score $s_{kl}(\mathbf{X}, y)$ on $\Upsilon^y$, where $\Upsilon^y$ is the subset of the calibration dataset with $\mathbf{Y} = y$ and $N_y = |\Upsilon^y|$. Then we predict the voxel $\mathbf{X}_{test}$ as occupied if $\exists y \in \mathcal{Y}_r, s_{kl}(\mathbf{X}_{test}, y) \leq q_o^y$.

**Semantic Level.** On the semantic level, we need to achieve the same class-balanced coverage under the geometric level coverage guarantee. For all voxels predicted as occupied in the previous step, we generate the prediction set $\mathcal{C}(\mathbf{X}_{test}) \subset \{2, ..., M\}$ to satisfy the guarantee:

$$\mathbb{P}(\mathbf{Y}_{test} \in \mathcal{C}(\mathbf{X}_{test}) | \mathbf{Y}_{test} = y, o = T) \geq 1 - \alpha_s^y. \tag{3}$$

The score function here is $s(\mathbf{X}, y) = 1 - f(\mathbf{X})_y$. We compute the quantile $q_s^y$ for class $y$ as the $\frac{\lceil (N_{yo}+1)(1-\alpha) \rceil}{N_{yo}}$ quantile of the score on $\Upsilon_o^y$, where $\Upsilon_o^y$ is the subset of the calibration dataset that has label $y$ and are predicted as occupied on the geometric level of our HCP. $N_{yo} = |\Upsilon_o^y|$. The prediction set is generated as:

$$\mathcal{C}(\mathbf{X}_{test}) = \{y : s_{kl}(\mathbf{X}, y) \leq q_o^y \wedge s(\mathbf{X}, y) \leq q_s^y\}. \tag{4}$$

**Proposition 1.** *For a desired error rate $\alpha^y$, we select $\alpha_o^y$ and $\alpha_s^y$ as $1 - \alpha^y = (1 - \alpha_s^y)(1 - \alpha_o^y)$, then the prediction set generated as Eq. 4 satisfies $\mathbb{P}(\mathbf{Y}_{test} \in \mathcal{C}(\mathbf{X}_{test}) | \mathbf{Y}_{test} = y) \geq 1 - \alpha^y$.*

The proof is in Appendix A.4.

## 4 Experiments

**OCC Model.** We assess the effectiveness of our approach through comprehensive experiments on three different OCC models: VoxFormer (Li et al. (2023b)), OccFormer (Zhang et al. (2023)) and CGFormer (Yu et al. (2024)). A detailed introduction to these three models is in Appendix A.2. **Dataset.** We use SemanticKITTI (Behley et al. (2019), with 20 classes) and KITTI360 (Li et al. (2023a), with 19 classes). (more details in Appendix A.5). Detailed experiment settings are in Appendix A.6. Experiments on the Occ3D-nuScenes (Caesar et al. (2020)) dataset are in Appendix A.9.

### 4.1 Uncertainty Propagation Performance

Table 1: Performance evaluation of our Depth-UP on three OCC models with two datasets. Values in parentheses indicate the improvement of our Depth-UP compared with the baseline.

| Dataset | OCC | Method | IoU ↑ | Precision ↑ | Recall ↑ | mIoU ↑ |
|---|---|---|---|---|---|---|
| SemanticKITTI | VoxFormer | Base | 44.02 | 62.32 | 59.99 | 12.35 |
| | | Our | 45.85 (+1.83) | 63.10 (+0.78) | 62.64 (+2.65) | 13.36 (+1.01) |
| | OccFormer | Base | 37.48 | 48.71 | 61.92 | 12.83 |
| | | Our | 41.64 (+4.16) | 53.99 (+5.28) | 64.54 (+2.62) | 14.56 (+1.73) |
| | CGFormer | Base | 44.92 | 60.91 | 63.12 | 15.82 |
| | | Our | 48.55 (+3.63) | 67.35 (+6.44) | 63.53 (+0.41) | 17.00 (+1.18) |
| KITTI360 | VoxFormer | Base | 38.76 | 57.67 | 54.18 | 11.91 |
| | | Our | 43.25 (+4.49) | 65.81 (+7.29) | 55.78 (+1.60) | 13.55 (+1.64) |

**Metric.** For OCC evaluation, we use intersection over union (IoU) to assess geometric completion, independent of semantics, as it is critical for obstacle avoidance in AVs. Semantic performance is measured by mean IoU (mIoU) across all classes. Given the strong negative correlation between IoU and mIoU (Li et al. (2023b)), an effective model must perform well on both metrics.

The experimental results of our Depth-UP on VoxFormer, OccFormer and CGFormer are presented in Table 1. As OccFormer is not available on KITTI360, we evaluate it with our Depth-UP only on SemanticKITTI. These results demonstrate that Depth-UP effectively leverages quantified uncertainty from the depth model to enhance OCC model performance, achieving up to a 4.49 (11.58%) improvement in IoU and up to a 1.73 (12.95%) improvement in mIoU, while also significantly improving both precision and recall in the geometry completion aspect of OCC. Even minor improvements in IoU and mIoU indicate meaningful progress in OCC performance (Zhang et al. (2023); Huang et al. (2023)). A detailed breakdown of mIoU results for each class is provided in Appendix A.7.

Figure 4 presents visualizations of the VoxFormer with and without our Depth-UP on SemanticKITTI. As highlighted by the orange dashed boxes, Depth-UP notably enhances the performance of OCC models in predicting rare classes, such as persons and bicyclists. Specifically, in the third row, Depth-UP successfully detects a person crossing the road at the corner, preventing a potential crash, while the baseline model fails to recognize this individual. By improving the detection of such critical instances, our Depth-UP significantly reduces the risk of injury to pedestrians and enhances the safety of autonomous vehicles. Additional visualization results can be found in Appendix A.7.

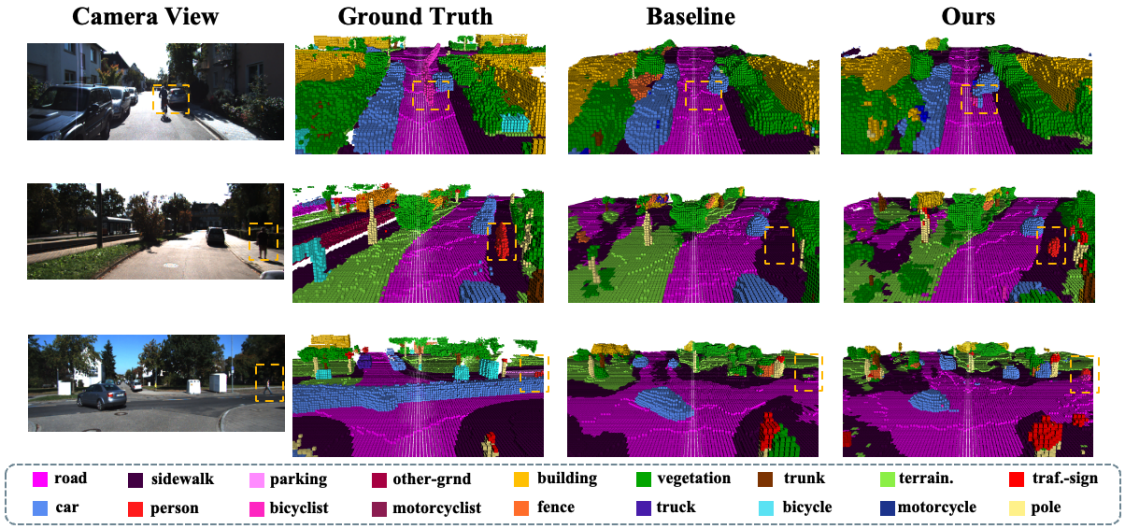


Figure 4: Qualitative results of the base VoxFormer model and that with our Depth-UP[1].

### 4.2 Uncertainty Quantification Performance

We evaluate our HCP on the geometric level and the final uncertainty quantification. Since we do not have the labeled test part of SemanticKITTI, we randomly split the original validation part of SemanticKITTI into the calibration dataset (take up 30%) and the test dataset (take up 70%). For KITTI360, we use the validation part as the calibration dataset and the test part as the test dataset.

**Geometric Level.** For the geometric level, the target of methods is to achieve the best trade-off between IoU and the occupied recall of rare classes. To show the effectiveness of our novel KL-based score function on the geometric level, we compare it with two common score functions in Angelopoulos & Bates (2021): class score $(1 - f(\mathbf{X})_y)$ and occupied score $(1 - \sum_{y=2}^{M} f(\mathbf{X})_y)$. Figure 5(a) shows the IoU results across different occupied recalls of the rare class person for different datasets. Figure 5(b) shows the IoU results across different occupied recalls of the rare class bicyclist for different basic OCC models. Here "Our Depth-UP" means the basic OCC model with our Depth-UP method. We can see that our KL-based score function always achieves the best geometry performance for the same occupied recall, compared with two baselines. Our HCP significantly outperforms baselines because it not only considers the occupied probability across all nonempty classes but also leverages the entire probability distribution.

To achieve the optimal balance between IoU and occupied recall, we can adjust the desired occupied recall. For instance, in the top right subfigure of Figure 5(a), the OCC without HCP shows an IoU of 45.85 and an occupied recall for the person class of 20.69. By setting the occupied recall to 21.75, the IoU improves to 45.94. Increasing the occupied recall beyond 30 (45.0% improvement) results in a decrease in IoU to 44.38 (3.4% reduction). This demonstrates that our HCP method can substantially boost the occupied recall of rare classes with a minor reduction in IoU.

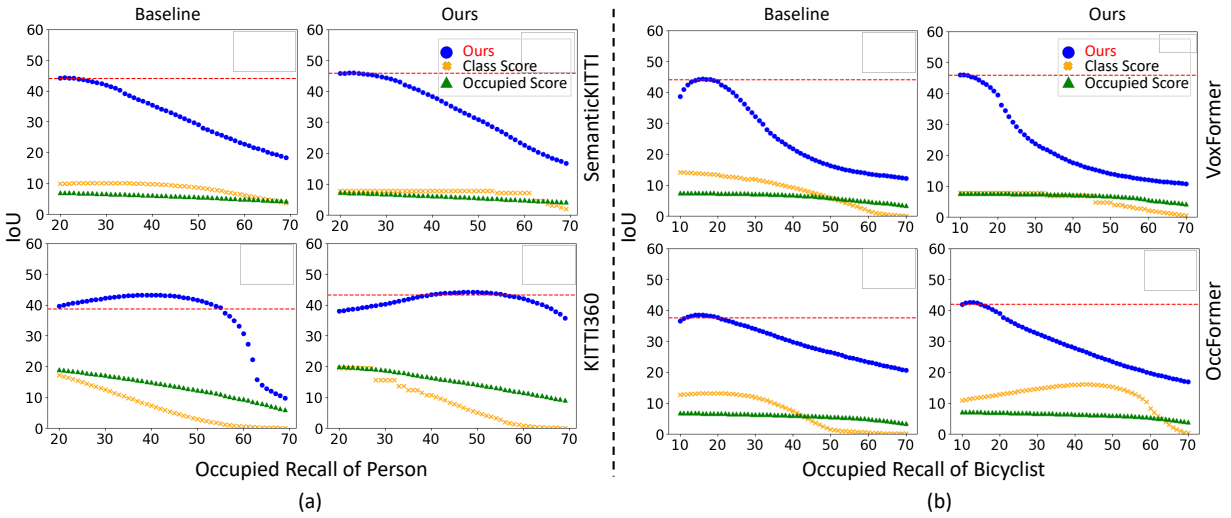


Figure 5: Compare our KL-based score function with the class and occupied scores. Evaluate OCC's geometry performance across different occupied recalls of the rare class. The red dotted line shows the IoU of the OCC without CP. (a): Results on the basic VoxFormer across different datasets for the person class. (b): Results on SemanticKITTI across different basic OCCs for the bicyclist class.

**Uncertainty Quantification.** To measure the quantified uncertainty of different CP methods, we usually use the average class coverage gap (CovGap) and average set size (AvgSize) of the prediction sets as metrics (Ding et al. (2024)). For a given class $y \in \mathcal{Y}\backslash\{1\}$ with the defined error rate $\alpha^y$, the empirical class-conditional coverage of class $y$ is $c_y = \frac{1}{|\Upsilon^y|}\sum_{i\in\Upsilon^y}\mathbb{I}\{\mathbf{Y}_i \in \mathcal{C}(\mathbf{X}_i)\}$. The CovGap is defined as $\frac{1}{|\mathcal{Y}|-1}\sum_{y\in\mathcal{Y}\backslash\{1\}}|c_y-(1-\alpha^y)|$. This measures how far the class-conditional coverage is from the desired coverage $1-\alpha^y$. The AvgSize is

[1]The incorrect ground truth in the third row occurs because SemanticKITTI uses LiDAR temporal fusion for annotations, which results in ghosting effects for dynamic objects.

defined as $\frac{1}{T}\sum_{i=1}^{T}|\mathcal{C}(\mathbf{X}_i)|$, where $T$ is the number of samples in the test dataset and $\mathcal{C}(\mathbf{X}_i)$ does not contain the empty class. A good UQ method should achieve both small CovGap and AvgSize.

Table 2 compares our HCP method with standard conformal prediction (SCP) and class-conditional conformal prediction (CCCP) on the SemanticKITTI dataset, as introduced in Subsection 3.2.1. For each class, the desired error rate is set by scaling the OCC model's original error rate by the scale $\lambda = 0.86$, raising the coverage requirement. The desired error rate of "Ours*" is the same as that on the base OCC model. The corresponding results on KITTI360 dataset can be found in Appendix A.8.

Our results demonstrate that HCP consistently achieves robust empirical class-conditional coverage and produces smaller prediction sets. In contrast, the performance of SCP and CCCP varies across different OCC models. Specifically, for our Depth-UP based on CGFormer, HCP reduces the set size by 90% and the coverage gap by 54%, compared to SCP. For our Depth-UP based on VoxFormer, HCP reduces the set size by 79% and the coverage gap by 64%, compared to CCCP. As noted in Subsection 3.2.1, SCP consistently fails to provide conditional coverage, although sometimes it provides a very small set size. Both SCP and CCCP tend to generate nonempty $C(\mathbf{X})$ for most voxels, potentially obstructing AVs. In contrast, HCP only generates nonempty $C(\mathbf{X})$ for these selected occupied voxels, thereby minimizing prediction set sizes while maintaining reliable class-conditional coverage. Moreover, under the same error rate setting, our HCP with the Depth-UP model (referred to as "Ours*") achieves the best UQ performance, reducing the set size by up to 18% under a similar coverage gap compared to applying HCP alone. This demonstrates that our $\alpha$-OCC framework, which integrates Depth-UP and HCP, achieves superior performance in both accuracy and UQ.

Table 2: For the SemanticKITTI, compare our HCP (referred to as "Ours") with standard conformal prediction (SCP) and class-conditional conformal prediction (CCCP) on CovGap and AvgSize. "Ours*" are results of our HCP + Depth-UP under the same defined error rate for the base model.

| Basic OCC | VoxFormer | | | | | | | OccFormer | | | | | | | CGFormer | | | | | | |
|---|---|---|---|---|---|---|---|---|---|---|---|---|---|---|---|---|---|---|---|---|---|
| Method | Base | | | Our Depth-UP | | | | Base | | | Our Depth-UP | | | | Base | | | Our Depth-UP | | | |
| CP | SCP | CCCP | Ours | Ours* | SCP | CCCP | Ours | SCP | CCCP | Ours | Ours* | SCP | CCCP | Ours | SCP | CCCP | Ours | Ours* | SCP | CCCP | Ours |
| CovGap ↓ | 0.22 | 0.03 | 0.04 | 0.04 | 0.26 | 0.11 | 0.04 | 0.26 | 0.03 | 0.04 | 0.04 | 0.31 | 0.04 | 0.03 | 0.22 | 0.03 | 0.02 | 0.03 | 0.16 | 0.03 | 0.03 |
| AvgSize ↓ | 1.53 | 1.71 | 1.13 | 0.93 | 0.97 | 6.43 | 1.36 | 0.10 | 3.42 | 0.94 | 0.80 | 0.10 | 2.96 | 1.24 | 3.63 | 3.00 | 1.67 | 1.33 | 5.19 | 3.31 | 1.72 |

### 4.3 Ablation Study

Table 3: Ablation study on our Depth-UP framework with VoxFormer and SemanticKITTI.

| PGC | PSS | IoU ↑ | Precision ↑ | Recall ↑ | mIoU ↑ | FPS ↑ |
|---|---|---|---|---|---|---|
| | | 44.02 | 62.32 | 59.99 | 12.35 | **8.85** |
| ✓ | | 44.91 | 63.76 | 60.30 | 12.58 | 7.14 |
| | ✓ | 44.40 | 62.69 | 60.35 | 12.77 | 8.76 |
| ✓ | ✓ | **45.85** | **63.10** | **62.64** | **13.36** | 7.08 |

**Uncertainty Propagation.** We conducted an ablation study to assess the contributions of each technique proposed in our Depth-UP, as detailed in Table 3. The best results are shown in bold. The results indicate that Propagation on Geometry Completion (PGC) significantly enhances IoU, precision, and recall, which are key metrics for geometry. This improvement demonstrates how probabilistic geometry projection effectively utilizes uncertainty during the geometry stage of OCC. Additionally, Propagation on Semantic Segmentation (PSS) markedly improves mIoU, a crucial metric for semantic accuracy, demonstrating that uncertainty is effectively leveraged in semantic segmentation through depth feature extraction. Notably, the combined application of both techniques yields performance improvements that surpass the sum of their individual contributions. This shows that uncertainty propagation in OCC completion and segmentation boosts performance. Additional results on the influence of depth mean can be found in Appendix A.7.

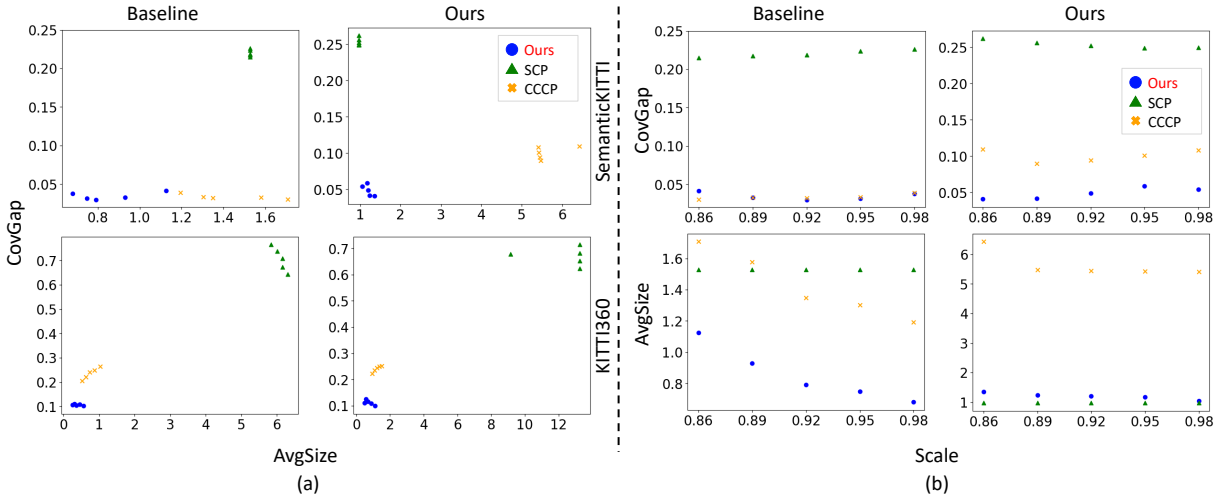


Figure 6: Compare our HCP with SCP and CCCP on CovGap and AvgSize with VoxFormer. Each point denotes a desired class error rate. Lower CovGap and AvgSize indicate better performance. (a): CovGap vs. AvgSize on different settings across different datasets. (b): CovGap vs. scale and AvgSize vs. scale on the SemanticKITTI where the scale represents the desired class error rate.

**Uncertainty Quantification.** We compare our HCP with SCP and CCCP under different desired class-specific error rate $\alpha^y$ settings with the basic VoxFormer, as shown in Figure 6. We consider five error rate scale settings with $\lambda \in \{0.86, 0.89, 0.92, 0.95, 0.98\}$. The points of our HCP are always located in the left bottom corner of subfigures in Figure 6(a) which means our HCP achieves the best performance on set size and coverage gap under all error rate settings. In Figure 6(b), our HCP always achieves low CovGap indicating it can always satisfy the coverage guarantee even under high requirements. SCP consistently has the largest CovGap due to its disregard for conditional coverage. While CCCP addresses this issue, it often results in a high AvgSize because it generates prediction sets for empty voxels. In contrast, our HCP method not only accounts for conditional coverage but also excludes empty voxels, generating prediction sets exclusively for predicted occupied voxels. For all CP approaches, as the desired error rate becomes smaller, the set size tends to be larger. CPs increase the set size to satisfy the coverage guarantee. The results on other OCC models are shown in Appendix A.8, where our HCP is applied to one LiDAR-based OCC to show its scalability.

**Limitation.** Our Depth-UP introduces a 20% reduction in FPS; however, this does not substantially impact the overall efficiency of OCC models. Notably, we did not apply any code-level optimization to improve runtime, indicating the added computational overhead is acceptable.

## 5 Conclusion

This paper introduces a novel approach to enhancing camera-based 3D Semantic Occupancy Prediction (OCC) by incorporating uncertainty inherent in models. Our proposed framework, $\alpha$-OCC, integrates the uncertainty propagation (Depth-UP) from depth models to improve OCC performance in both geometry completion and semantic segmentation. A novel hierarchical conformal prediction (HCP) method is designed to quantify OCC uncertainty effectively under high-level class imbalance. Our extensive experiments demonstrate the effectiveness of $\alpha$-OCC. The Depth-UP significantly improves prediction accuracy, achieving up to 11.58% increase in IoU and up to 12.95% increase in mIoU. The HCP significantly improves performance by ensuring robust class-conditional coverage while keeping compact prediction sets. Compared to baselines, it achieves up to 90% reduction in set size and decreases the coverage gap by up to 64%. Additionally, integrating HCP with Depth-UP further reduces the set size by 18%. These results highlight the significant improvements in both accuracy and uncertainty quantification offered by our approach, especially for rare safety-critical classes, such as persons and bicyclists, thereby reducing potential risks for AVs. In the future, we will extend HCP to other highly imbalanced classification tasks.

## References


Anastasios N Angelopoulos and Stephen Bates. A gentle introduction to conformal prediction and distribution-free uncertainty quantification. *arXiv preprint arXiv:2107.07511*, 2021.

George B Arfken, Hans J Weber, and Frank E Harris. *Mathematical methods for physicists: a comprehensive guide*. Academic press, 2011.

Vijay Badrinarayanan, Alex Kendall, and Roberto Cipolla. Segnet: A deep convolutional encoder-decoder architecture for image segmentation. *IEEE transactions on pattern analysis and machine intelligence*, 39 (12):2481–2495, 2017.

Jens Behley, Martin Garbade, Andres Milioto, Jan Quenzel, Sven Behnke, Cyrill Stachniss, and Jurgen Gall. Semantickitti: A dataset for semantic scene understanding of lidar sequences. In *Proceedings of the IEEE/CVF international conference on computer vision*, pp. 9297–9307, 2019.

Shariq Farooq Bhat, Ibraheem Alhashim, and Peter Wonka. Adabins: Depth estimation using adaptive bins. In *Proceedings of the IEEE/CVF conference on computer vision and pattern recognition*, pp. 4009–4018, 2021.

Mateusz Buda, Atsuto Maki, and Maciej A Mazurowski. A systematic study of the class imbalance problem in convolutional neural networks. *Neural networks*, 106:249–259, 2018.

Holger Caesar, Varun Bankiti, Alex H Lang, Sourabh Vora, Venice Erin Liong, Qiang Xu, Anush Krishnan, Yu Pan, Giancarlo Baldan, and Oscar Beijbom. nuscenes: A multimodal dataset for autonomous driving. In *Proceedings of the IEEE/CVF conference on computer vision and pattern recognition*, pp. 11621–11631, 2020.

Anh-Quan Cao and Raoul De Charette. Monoscene: Monocular 3d semantic scene completion. In *Proceedings of the IEEE/CVF Conference on Computer Vision and Pattern Recognition*, pp. 3991–4001, 2022.

Anh-Quan Cao, Angela Dai, and Raoul de Charette. Pasco: Urban 3d panoptic scene completion with uncertainty awareness. In *Proceedings of the IEEE/CVF Conference on Computer Vision and Pattern Recognition*, pp. 14554–14564, 2024.

Robin Chan, Matthias Rottmann, Fabian Hüger, Peter Schlicht, and Hanno Gottschalk. Application of decision rules for handling class imbalance in semantic segmentation. *arXiv preprint arXiv:1901.08394*, 2019.

Bike Chen, Chen Gong, and Jian Yang. Importance-aware semantic segmentation for autonomous vehicles. *IEEE Transactions on Intelligent Transportation Systems*, 20(1):137–148, 2018.

Ran Cheng, Christopher Agia, Yuan Ren, Xinhai Li, and Liu Bingbing. S3cnet: A sparse semantic scene completion network for lidar point clouds. In *Conference on Robot Learning*, pp. 2148–2161. PMLR, 2021.

Tiffany Ding, Anastasios Angelopoulos, Stephen Bates, Michael Jordan, and Ryan J Tibshirani. Class-conditional conformal prediction with many classes. *Advances in Neural Information Processing Systems*, 36, 2024.

David Eigen and Rob Fergus. Predicting depth, surface normals and semantic labels with a common multi-scale convolutional architecture. In *Proceedings of the IEEE international conference on computer vision*, pp. 2650–2658, 2015.

Abdelrahman Eldesokey, Michael Felsberg, Karl Holmquist, and Michael Persson. Uncertainty-aware cnns for depth completion: Uncertainty from beginning to end. In *Proceedings of the IEEE/CVF Conference on Computer Vision and Pattern Recognition*, pp. 12014–12023, 2020.

Di Feng, Ali Harakeh, Steven L Waslander, and Klaus Dietmayer. A review and comparative study on probabilistic object detection in autonomous driving. *IEEE Transactions on Intelligent Transportation Systems*, 23(8):9961–9980, 2021.

Andreas Geiger, Philip Lenz, and Raquel Urtasun. Are we ready for autonomous driving? the kitti vision benchmark suite. In *2012 IEEE conference on computer vision and pattern recognition*, pp. 3354–3361. IEEE, 2012.

Chuan Guo, Geoff Pleiss, Yu Sun, and Kilian Q Weinberger. On calibration of modern neural networks. In *International conference on machine learning*, pp. 1321–1330. PMLR, 2017.

Kaiming He, Xiangyu Zhang, Shaoqing Ren, and Jian Sun. Deep residual learning for image recognition. In *Proceedings of the IEEE conference on computer vision and pattern recognition*, pp. 770–778, 2016.

Sihong He, Songyang Han, Sanbao Su, Shuo Han, Shaofeng Zou, and Fei Miao. Robust multi-agent reinforcement learning with state uncertainty. *arXiv preprint arXiv:2307.16212*, 2023.

Yihan Hu, Jiazhi Yang, Li Chen, Keyu Li, Chonghao Sima, Xizhou Zhu, Siqi Chai, Senyao Du, Tianwei Lin, Wenhai Wang, et al. Planning-oriented autonomous driving. In *Proceedings of the IEEE/CVF Conference on Computer Vision and Pattern Recognition*, pp. 17853–17862, 2023.

Yuanhui Huang, Wenzhao Zheng, Yunpeng Zhang, Jie Zhou, and Jiwen Lu. Tri-perspective view for vision-based 3d semantic occupancy prediction. In *Proceedings of the IEEE/CVF conference on computer vision and pattern recognition*, pp. 9223–9232, 2023.

Yuanhui Huang, Wenzhao Zheng, Borui Zhang, Jie Zhou, and Jiwen Lu. Selfocc: Self-supervised vision-based 3d occupancy prediction. In *Proceedings of the IEEE/CVF Conference on Computer Vision and Pattern Recognition (CVPR)*, pp. 19946–19956, June 2024.

Ashkan M Jasour and Brian C Williams. Risk contours map for risk bounded motion planning under perception uncertainties. In *Robotics: Science and Systems*, pp. 22–26, 2019.

Balaji Lakshminarayanan, Alexander Pritzel, and Charles Blundell. Simple and scalable predictive uncertainty estimation using deep ensembles. *Advances in neural information processing systems*, 30, 2017.

Yiming Li, Sihang Li, Xinhao Liu, Moonjun Gong, Kenan Li, Nuo Chen, Zijun Wang, Zhiheng Li, Tao Jiang, Fisher Yu, et al. Sscbench: A large-scale 3d semantic scene completion benchmark for autonomous driving. *arXiv preprint arXiv:2306.09001*, 2023a.

Yiming Li, Zhiding Yu, Christopher Choy, Chaowei Xiao, Jose M Alvarez, Sanja Fidler, Chen Feng, and Anima Anandkumar. Voxformer: Sparse voxel transformer for camera-based 3d semantic scene completion. In *Proceedings of the IEEE/CVF conference on computer vision and pattern recognition*, pp. 9087–9098, 2023b.

Yinhao Li, Han Bao, Zheng Ge, Jinrong Yang, Jianjian Sun, and Zeming Li. Bevstereo: Enhancing depth estimation in multi-view 3d object detection with temporal stereo. In *Proceedings of the AAAI Conference on Artificial Intelligence*, volume 37, pp. 1486–1494, 2023c.

Zhiqi Li, Wenhai Wang, Hongyang Li, Enze Xie, Chonghao Sima, Tong Lu, Yu Qiao, and Jifeng Dai. Bevformer: Learning bird's-eye-view representation from multi-camera images via spatiotemporal transformers. In *European conference on computer vision*, pp. 1–18. Springer, 2022.

Yiyi Liao, Jun Xie, and Andreas Geiger. Kitti-360: A novel dataset and benchmarks for urban scene understanding in 2d and 3d. *IEEE Transactions on Pattern Analysis and Machine Intelligence*, 45(3): 3292–3310, 2022.

Tsung-Yi Lin, Priya Goyal, Ross Girshick, Kaiming He, and Piotr Dollár. Focal loss for dense object detection. In *Proceedings of the IEEE international conference on computer vision*, pp. 2980–2988, 2017.

Yan Lu, Xinzhu Ma, Lei Yang, Tianzhu Zhang, Yating Liu, Qi Chu, Junjie Yan, and Wanli Ouyang. Geometry uncertainty projection network for monocular 3d object detection. In *Proceedings of the IEEE/CVF International Conference on Computer Vision*, pp. 3111–3121, 2021.

Laurent Lucas, Céline Loscos, and Yannick Remion. Camera calibration: geometric and colorimetric correction. *3D Video: From Capture to Diffusion*, pp. 91–112, 2013.

Qihang Ma, Xin Tan, Yanyun Qu, Lizhuang Ma, Zhizhong Zhang, and Yuan Xie. Cotr: Compact occupancy transformer for vision-based 3d occupancy prediction. In *Proceedings of the IEEE/CVF Conference on Computer Vision and Pattern Recognition (CVPR)*, pp. 19936–19945, June 2024.

Fadel M Megahed, Ying-Ju Chen, Aly Megahed, Yuya Ong, Naomi Altman, and Martin Krzywinski. The class imbalance problem. *Nat Methods*, 18(11):1270–7, 2021.

Gregory P Meyer and Niranjan Thakurdesai. Learning an uncertainty-aware object detector for autonomous driving. In *2020 IEEE/RSJ International Conference on Intelligent Robots and Systems (IROS)*, pp. 10521–10527. IEEE, 2020.

Dimity Miller, Lachlan Nicholson, Feras Dayoub, and Niko Sünderhauf. Dropout sampling for robust object detection in open-set conditions. In *2018 IEEE International Conference on Robotics and Automation (ICRA)*, pp. 3243–3249. IEEE, 2018.

Mingjie Pan, Jiaming Liu, Renrui Zhang, Peixiang Huang, Xiaoqi Li, Hongwei Xie, Bing Wang, Li Liu, and Shanghang Zhang. Renderocc: Vision-centric 3d occupancy prediction with 2d rendering supervision. In *2024 IEEE International Conference on Robotics and Automation (ICRA)*, pp. 12404–12411. IEEE, 2024.

Jonah Philion and Sanja Fidler. Lift, splat, shoot: Encoding images from arbitrary camera rigs by implicitly unprojecting to 3d. In *Computer Vision–ECCV 2020: 16th European Conference, Glasgow, UK, August 23–28, 2020, Proceedings, Part XIV 16*, pp. 194–210. Springer, 2020.

Matteo Poggi, Filippo Aleotti, Fabio Tosi, and Stefano Mattoccia. On the uncertainty of self-supervised monocular depth estimation. In *Proceedings of the IEEE/CVF Conference on Computer Vision and Pattern Recognition*, pp. 3227–3237, 2020.

Fiana Raiber and Oren Kurland. Kullback-leibler divergence revisited. In *Proceedings of the ACM SIGIR international conference on theory of information retrieval*, pp. 117–124, 2017.

Luis Roldao, Raoul de Charette, and Anne Verroust-Blondet. Lmscnet: Lightweight multiscale 3d semantic completion. In *2020 International Conference on 3D Vision (3DV)*, pp. 111–119. IEEE, 2020.

Faranak Shamsafar, Samuel Woerz, Rafia Rahim, and Andreas Zell. Mobilestereonet: Towards lightweight deep networks for stereo matching. In *Proceedings of the ieee/cvf winter conference on applications of computer vision*, pp. 2417–2426, 2022.

Shuran Song, Fisher Yu, Andy Zeng, Angel X Chang, Manolis Savva, and Thomas Funkhouser. Semantic scene completion from a single depth image. In *Proceedings of the IEEE conference on computer vision and pattern recognition*, pp. 1746–1754, 2017.

Sanbao Su, Yiming Li, Sihong He, Songyang Han, Chen Feng, Caiwen Ding, and Fei Miao. Uncertainty quantification of collaborative detection for self-driving. In *2023 IEEE International Conference on Robotics and Automation (ICRA)*, pp. 5588–5594. IEEE, 2023.

Sanbao Su, Songyang Han, Yiming Li, Zhili Zhang, Chen Feng, Caiwen Ding, and Fei Miao. Collaborative multi-object tracking with conformal uncertainty propagation. *IEEE Robotics and Automation Letters*, 2024.

Sanbao Su, Xin Li, Thang Doan, Sima Behpour, Wenbin He, Liang Gou, Fei Miao, and Liu Ren. Metaat: Active testing for label-efficient evaluation of dense recognition tasks. In *European Conference on Computer Vision*, pp. 325–342. Springer, 2025.

Junjiao Tian, Yen-Cheng Liu, Nathaniel Glaser, Yen-Chang Hsu, and Zsolt Kira. Posterior re-calibration for imbalanced datasets. *Advances in neural information processing systems*, 33:8101–8113, 2020.

Xiaoyu Tian, Tao Jiang, Longfei Yun, Yucheng Mao, Huitong Yang, Yue Wang, Yilun Wang, and Hang Zhao. Occ3d: A large-scale 3d occupancy prediction benchmark for autonomous driving. *Advances in Neural Information Processing Systems*, 36, 2024.

Jason Van Hulse, Taghi M Khoshgoftaar, and Amri Napolitano. Experimental perspectives on learning from imbalanced data. In *Proceedings of the 24th international conference on Machine learning*, pp. 935–942, 2007.

Antonin Vobecky, Oriane Siméoni, David Hurych, Spyridon Gidaris, Andrei Bursuc, Patrick Pérez, and Josef Sivic. Pop-3d: Open-vocabulary 3d occupancy prediction from images. *Advances in Neural Information Processing Systems*, 36, 2024.

Lele Wang and Yingping Huang. A survey of 3d point cloud and deep learning-based approaches for scene understanding in autonomous driving. *IEEE Intelligent Transportation Systems Magazine*, 14(6):135–154, 2021.

Yuqi Wang, Yuntao Chen, and Zhaoxiang Zhang. Frustumformer: Adaptive instance-aware resampling for multi-view 3d detection. In *Proceedings of the IEEE/CVF Conference on Computer Vision and Pattern Recognition*, pp. 5096–5105, 2023.

Yuqi Wang, Yuntao Chen, Xingyu Liao, Lue Fan, and Zhaoxiang Zhang. Panoocc: Unified occupancy representation for camera-based 3d panoptic segmentation. In *Proceedings of the IEEE/CVF conference on computer vision and pattern recognition*, pp. 17158–17168, 2024.

Songlin Wei, Haoran Geng, Jiayi Chen, Congyue Deng, Cui Wenbo, Chengyang Zhao, Xiaomeng Fang, Leonidas Guibas, and He Wang. D3roma: Disparity diffusion-based depth sensing for material-agnostic robotic manipulation. In *ECCV 2024 Workshop on Wild 3D: 3D Modeling, Reconstruction, and Generation in the Wild*, 2024.

Wenda Xu, Jia Pan, Junqing Wei, and John M Dolan. Motion planning under uncertainty for on-road autonomous driving. In *2014 IEEE International Conference on Robotics and Automation (ICRA)*, pp. 2507–2512. IEEE, 2014.

Zhu Yu, Runmin Zhang, Jiacheng Ying, Junchen Yu, Xiaohai Hu, Lun Luo, Si-Yuan Cao, and Hui-Liang Shen. Context and geometry aware voxel transformer for semantic scene completion. *arXiv preprint arXiv:2405.13675*, 2024.

Yunpeng Zhang, Zheng Zhu, and Dalong Du. Occformer: Dual-path transformer for vision-based 3d semantic occupancy prediction. In *Proceedings of the IEEE/CVF International Conference on Computer Vision*, pp. 9433–9443, 2023.

Zhengyou Zhang. A flexible new technique for camera calibration. *IEEE Transactions on pattern analysis and machine intelligence*, 22(11):1330–1334, 2000.

# A Appendix

## A.1 More Related Work

**Class Imbalance.** In real-world applications like robotics and autonomous vehicles (AVs), datasets often face the challenge of class imbalance (Chen et al. (2018)). Rare classes, typically encompassing high safety-critical entities such as persons, are significantly outnumbered by lower safety-critical classes like trees and buildings. Various strategies have been proposed to tackle class imbalance. Data-level methods involve random under-sampling of majority classes and over-sampling of minority classes during training (Van Hulse et al. (2007)). However, they struggle to address the pronounced class imbalance encountered in OCC (Megahed et al. (2021)), as shown in Section 1. Algorithm-level methods employ cost-sensitive losses to adjust the training process for different tasks, such as depth estimation (Eigen & Fergus (2015)) and 2D segmentation (Badrinarayanan et al. (2017)). While algorithm-level methods have been widely implemented in current OCC models (Voxformer Li et al. (2023b) utilizes Focal Loss Lin et al. (2017) as the loss function), they still fall short in accurately predicting minority classes. In contrast, classifier-level methods postprocess output class probabilities during the testing phase through posterior calibration (Buda et al. (2018); Tian et al. (2020)). In this paper, we propose a hierarchical conformal prediction method falling within this category, aimed at enhancing the recall of rare safety-critical classes in the OCC task.

## A.2 Introduction on Semantic Occupancy Prediction Models

**Semantic Occupancy Prediction.** The concept of 3D Semantic Occupancy Prediction (OCC), which is also known as 3D semantic scene completion, was first introduced by SSCNet (Song et al. (2017)), integrating both geometric and semantic reasoning. Since its inception, numerous studies have emerged, categorized into two streams: LiDAR-based OCC (Roldao et al. (2020); Cheng et al. (2021)) and camera-based OCC (Cao & De Charette (2022); Li et al. (2023b); Zhang et al. (2023); Huang et al. (2024); Vobecky et al. (2024)).

Recently, camera-based OCC has gained increasing attention due to its advantages in visual recognition and cost-effectiveness (Ma et al. (2024)). Depth predictions from depth models are instrumental in projecting 2D information into 3D space for it. Existing methodologies can be classified into two paradigms based on their utilization of depth information: 3D-to-2D querying and 2D-to-3D lifting. The former Li et al. (2023b; 2022) generates query proposals using depth estimation and leverages them to extract rich visual features from the 3D scene. The latter Tian et al. (2024); Zhang et al. (2023); Yu et al. (2024), meanwhile, projects multi-view 2D image features into depth-aware frustums, as proposed by LSS Philion & Fidler (2020).

However, these methods overlook depth estimation uncertainty. Despite leveraging latent depth distribution, 2D-to-3D lifting technique sacrifices precise information and neglects lens distortion issues during geometry completion (Lucas et al. (2013)). To address this, we propose an uncertainty propagation framework from depth models to enhance OCC performance.

During the experiments, we used three OCC models: VoxFormer (Li et al. (2023b)), OccFormer (Zhang et al. (2023)) and CGFormer (Yu et al. (2024)). VoxFormer is the 3D-to-2D querying approach. OccFormer and CGFormer are the 2D-to-3D lifting approaches. So we have considered both paradigms that utilize depth information on OCC models in our experiments.

## A.3 Algorithm of HCP

Algo. 1 shows the detailed algorithm of our hierarchical conformal prediction (HCP).

## A.4 Proof of Proposition 1

**Proposition 1.** For a desired $\alpha^y$ value, we select $\alpha_o^y$ and $\alpha_s^y$ as $1-\alpha^y = (1-\alpha_s^y)(1-\alpha_o^y)$, then the prediction set generated as Eq. 4 satisfies that $\mathbb{P}(\mathbf{Y}_{test} \in \mathcal{C}(\mathbf{X}_{test}) | \mathbf{Y}_{test} = y) \geq 1-\alpha^y$.

*Proof.*

$$
\begin{aligned}
&\mathbb{P}(\mathbf{Y}_{test} \in \mathcal{C}(\mathbf{X}_{test})|\mathbf{Y}_{test} = y) = \sum_{o} \mathbb{P}(\mathbf{Y} \in \mathcal{C}(\mathbf{X})_{test})|\mathbf{Y}_{test} = y, o)\mathbb{P}(o|\mathbf{Y}_{test} = y) \\
=&\mathbb{P}(\mathbf{Y}_{test} \in \mathcal{C}(\mathbf{X}_{test})|\mathbf{Y}_{test} = y, o = T)\mathbb{P}(o = T|\mathbf{Y}_{test} = y) \\
&+ \mathbb{P}(\mathbf{Y}_{test} \in \mathcal{C}(\mathbf{X}_{test})|\mathbf{Y}_{test} = y, o = F)\mathbb{P}(o = F|\mathbf{Y}_{test} = y) \\
=&\mathbb{P}(\mathbf{Y}_{test} \in \mathcal{C}(\mathbf{X}_{test})|\mathbf{Y}_{test} = y, o = T)\mathbb{P}(o = T|\mathbf{Y}_{test} = y) \geq (1 - \alpha_s^y)(1 - \alpha_o^y) \\
\Rightarrow&\mathbb{P}(\mathbf{Y}_{test} \in \mathcal{C}(\mathbf{X}_{test})|\mathbf{Y}_{test} = y) \geq 1 - \alpha^y, \texttt{when } 1 - \alpha^y = (1 - \alpha_s^y)(1 - \alpha_o^y)
\end{aligned}
$$

□

**Algorithm 1:** Our Hierarchical Conformal Prediction (HCP)

**Data:** number of classes is $M$, calibration dataset $\mathcal{D}_{cali}(\mathbf{X}, \mathbf{Y})$ with $N$ samples, test dataset $\mathcal{D}_{test}(\mathbf{X})$ with $T$ samples, the considered rare class set $\mathcal{Y}_r$, the occupied error rate $\alpha_o^y$ $\forall y \in \mathcal{Y}_r$ ,desired class-specifical error rate $\alpha^y$ $\forall y \in \mathcal{Y}\backslash\{1\}$, the OCC model $f$.

**Result:** Prediction set $\mathcal{C}(\mathbf{X}_i)$, $\forall \mathbf{X}_i \in \mathcal{D}_{test}$

```
/* Calibration Step:  Geometric Level                                   */
```
$\mathcal{S}^y = \emptyset$ $\forall y \in \mathcal{Y}_r$; $\mathbf{O} = \{\varepsilon, 1, ..., 1\}^M$;

**for** $(\mathbf{X}_i, \mathbf{Y}_i) \in \mathcal{D}_{cali}$ **do**

  $s_{kl}(\mathbf{X}, y) = \mathrm{D}_{kl}(f(\mathbf{X}_i)||\mathbf{O})$ $y = \mathbf{Y}_i \in \mathcal{Y}_r$ as Eq. 2; add $s_{kl}(\mathbf{X}, y)$ into $\mathcal{S}^y$;

**end**

$q_o^y = \mathrm{Quantile}(\frac{\lceil (N_y+1)(1-\alpha_o^y) \rceil}{N_y}, \mathcal{S}^y)$ where $N_y = |\mathcal{S}^y|$, $\forall y \in \mathcal{Y}_r$;

```
/* Calibration Step:  Semantic Level                                    */
```
$\mathcal{S}_o^y = \emptyset$, $tp_y = 0$ and $fn_y = 0$ $\forall y \in \mathcal{Y}\backslash\{1\}$;

**for** $(\mathbf{X}_i, \mathbf{Y}_i) \in \mathcal{D}_{cali}$ *and* $\mathbf{Y}_i \in \mathcal{Y}\backslash\{1\}$ **do**

  **if** $\exists y \in \mathcal{Y}_r$, $s_{kl}(\mathbf{X}_i, y) \leq q_o^y$ **then**

    add $1 - f(\mathbf{X}_i)_{\mathbf{Y}_i}$ into $\mathcal{S}_o^{\mathbf{Y}_i}$ and $tp_{\mathbf{Y}_i} = tp_{\mathbf{Y}_i} + 1$;

  **else**

    $fn_{\mathbf{Y}_i} = fn_{\mathbf{Y}_i} + 1$;

  **end**

**end**

**for** $y \in \mathcal{Y}\backslash\{1\}$ **do**

  $\alpha_o^y = 1 - \frac{tp_y}{tp_y + fn_y}$ if $y \notin \mathcal{Y}_r$

  $\alpha_s^y = 1 - \frac{1-\alpha^y}{1-\alpha_o^y}$; $q_s^y = \mathrm{Quantile}(\frac{\lceil (N_{yo}+1)(1-\alpha_s^y) \rceil}{N_{yo}}, \mathcal{S}_o^y)$ where $N_o^y = |\mathcal{S}_o^y|$

**end**

```
/* Test Step                                                            */
```
**for** $\mathbf{X}_i \in \mathcal{D}_{test}$ **do**

  **if** $\exists y \in \mathcal{Y}_r$, $s_{kl}(\mathbf{X}, y) \leq q_o^y$ **then**

    $\mathcal{C}(\mathbf{X}_i) = \{y : 1 - f(\mathbf{X}_i)_y \leq q_s^y\}$

  **else**

    $\mathcal{C}(\mathbf{X}_i) = \emptyset$ which means it is empty class.

  **end**

**end**

### A.5 Introduction on Datasets

During the experiments, we used two datasets: SemanticKITTI (Behley et al. (2019)) and KITTI360 (Li et al. (2023a)). SemanticKITTI provides dense semantic annotations for each LiDAR sweep composed of 22 outdoor driving scenarios based on the KITTI Odometry Benchmark (Geiger et al. (2012)). Regarding the sparse input to an OCC model, it can be either a single voxelized LiDAR sweep or an RGB image. The voxel

grids are labeled with 20 classes (19 semantics and 1 empty), with the size of 0.2m $\times$ 0.2m $\times$ 0.2m. We only used the train and validation parts of SemanticKITTI as the annotations of the test part are not available. SSCBench-KITTI-360 provides dense semantic annotations for each image based on KITTI360 (Liao et al. (2022)), which is also called KITTI360 for simplification. The voxel grids are labeled with 19 classes (18 semantics and 1 empty), with the size of 0.2m $\times$ 0.2m $\times$ 0.2m. Both SemanticKITTI and KITTI360 are interested in a volume of 51.2m ahead of the car, 25.6m to left and right side, and 6.4m in height.

### A.6 Experimental Setting

We used two different servers to conduct experiments on the SemanticKITTI and KITTI360 datasets. For the SemanticKITTI dataset, we employed a system equipped with four NVIDIA Quadro RTX 8000 GPUs, each providing 48GB of VRAM. The system was configured with 128GB of system RAM. The training process required approximately 30 minutes per epoch, culminating in a total training duration of around 16 hours for 30 epochs. The software environment included the Linux operating system (version 18.04), Python 3.8.19, CUDA 11.1, PyTorch 1.9.1+cu111, and CuDNN 8.0.5.

For the KITTI360 dataset, we used a different system equipped with eight NVIDIA GeForce RTX 4090 GPUs, each providing 24GB of VRAM, with 720GB of system RAM. The training process required approximately 15 minutes per epoch, culminating in a total training duration of around 8 hours for 30 epochs. The software environment comprised the Linux operating system(version 18.04), Python 3.8.16, CUDA 11.1, PyTorch 1.9.1+cu111, and CuDNN 8.0.5. These settings ensure the reproducibility of our experiments on similar hardware configurations.

In our training, we used the AdamW optimizer with a learning rate of 2e-4 and a weight decay of 0.01. The learning rate schedule followed a Cosine Annealing policy with a linear warmup for the first 500 iterations, starting at a warmup ratio of $\frac{1}{3}$. The minimum learning rate ratio was set to 1e-3. We applied gradient clipping with a maximum norm of 35 to stabilize the training.

The user-defined target error rate $\alpha^y$ for each class $y$ is decided according to the prediction error rate of the original model. For each class, It is set by multiplying the original prediction error rate of OCC models with the scale $\lambda < 1$, which raises the coverage requirement. For example, for the person class, if the original model has 90% prediction error rate and we set the scale $\lambda = 0.9$, the user-defined target error rate $\alpha^{person}$ of person is decided as $90\% * 0.9 = 81\%$.

### A.7 More Results on Depth-UP

Table 5 presents a comparative analysis of our Depth-UP models against various OCC models, providing detailed mIoU results for different classes. Our Depth-UP demonstrates superior performance in geometry completion and semantic segmentation, outperforming all other OCC models and even surpassing LiDAR-based OCC models on the SemanticKITTI dataset. The VoxFormer with our Depth-UP achieves the best IoU on SemanticKITTI and the OccFormer with our Depth-UP achieves the best mIoU on SemanticKITTI. This improvement is attributed to propagating the inherent uncertainty of the depth model into both geometry completion and semantic segmentation of OCCs. Notably, on the KITTI360 dataset, our Depth-UP achieves the highest mIoU for bicycle, motorcycle, and person classes, which are crucial for safety.

For the person and bicyclist categories on the SemanticKITTI dataset, our Depth-UP decreases the mIoU. This issue primarily stems from annotation defects, particularly for dynamic objects such as persons and bicyclists. The SemanticKITTI dataset generates annotations using LiDAR temporal fusion, which introduces ghosting effects for moving objects. This problem has been documented in Figure 2 of the SSCBench (Li et al. (2023a)). While cars are also affected, most are stationary, so the impact is minimal. However, nearly all persons and bicyclists in the SemanticKITTI validation set are moving, leading to erroneous annotations. SSCBench has acknowledged this issue, and thus KITTI360 proposed in SSCBench does not suffer from ghosting problems. Our Depth-UP shows mIoU improvements in both person and bicyclist categories on KITTI360, aligning with our expectations. This may also explain why our Depth-UP enhances VoxFormer significantly more on KITTI360 compared to SemanticKITTI, showing a 1.64 mIoU improvement versus a 1.01 mIoU improvement.

**Visualization.** Figure 7 provides additional visualizations of the OCC model's performance with and without our Depth-UP on the SemanticKITTI dataset. These visualizations demonstrate that our Depth-UP enhances the model's ability to predict rare classes, such as persons and bicyclists, which are highlighted with orange dashed boxes. Notably, in the fourth row, our Depth-UP successfully predicts the presence of a person far from the camera, whereas the baseline model fails to do so. This indicates that Depth-UP improves object prediction in distant regions. By enhancing the detection of such critical objects, our Depth-UP significantly reduces the risk of accidents, thereby improving the safety of autonomous vehicles.

**Ablation Study.** We further conducted the ablation study on the influence of depth information on the semantic feature part of our Depth-UP framework, as shown in Table 4. When Propagation on Geometry Completion (PGC) is not applied, using only the depth mean in the Propagation on Semantic Segmentation (PSS, second row) improves IoU by 0.85 and mIoU by 0.16. When PGC is applied, compared to using only PGC (fourth row), incorporating only the depth mean in PSS (fifth row) increases IoU by 0.45 and mIoU by 0.08. These results indicate that the depth mean enhances geometric performance (IoU) and slightly improves semantic performance (mIoU). In contrast, incorporating depth uncertainty into PSS further improves mIoU by 0.26 when PGC is not applied and by 0.7 when PGC is applied. This demonstrates that leveraging depth uncertainty in PSS significantly enhances semantic performance. The depth mean primarily accounts for the improvement in IoU, suggesting a partial decoupling of the effects of uncertainty. One additional observation is that when PGC is not applied, PSS with only the depth mean achieves a higher IoU than the complete PSS, due to an imbalance in precision and recall. However, since the complete Depth-UP achieves the best performance in both IoU and mIoU across all settings, incorporating depth uncertainty into semantic features remains essential for optimal performance.

**Discussion.** The depth mean estimation $\hat{\mathbf{D}}$ in our OCC model remains identical to that in the corresponding base OCC model, as we only retrained the additional regression head for $\hat{\mathbf{\Sigma}}$ in the depth model. The improvement achieved by our OCC model does not result from nonexistent enhancements to the depth mean estimation; rather, it arises from effectively incorporating the uncertainty of depth estimation into the OCC models.

Table 4: Ablation study on the depth information for our Depth-UP framework with VoxFormer and SemanticKITTI.

| PGC | PSS | IoU ↑ | Precision ↑ | Recall ↑ | mIoU ↑ | FPS ↑ |
|---|---|---|---|---|---|---|
| | | 44.02 | 62.32 | 59.99 | 12.35 | **8.85** |
| | mean | 44.87 | 59.8 | 64.25 | 12.51 | 8.77 |
| | mean & std | 44.40 | 62.69 | 60.35 | 12.77 | 8.76 |
| ✓ | | 44.91 | 63.76 | 60.30 | 12.58 | 7.14 |
| ✓ | mean | 45.36 | 62.76 | 62.06 | 12.66 | 7.08 |
| ✓ | mean & std | **45.85** | **63.10** | **62.64** | **13.36** | 7.08 |

### A.8 More Results on HCP

Similar to Table 2, we compare our HCP method with standard conformal prediction (SCP) and class-conditional conformal prediction (CCCP) on the KITTI-360 dataset in Table 6. For each class, the desired error rate is obtained by scaling the original error rate of the OCC model using a factor of $\lambda = 0.86$, thereby increasing the coverage requirement. The desired error rate for "Ours*" remains identical to that of the base OCC model. Our results demonstrate that HCP consistently achieves robust empirical class-conditional coverage while producing significantly smaller prediction sets. In contrast, the performance of SCP and CCCP varies across different OCC models. Specifically, for our Depth-UP model based on VoxFormer, HCP reduces the prediction set size by 92% and the coverage gap by 84% compared to SCP. For the base VoxFormer model, HCP reduces the set size by 62% and the coverage gap by 46% compared to CCCP.

**More Discussion.** Our HCP significantly outperforms baselines because it not only considers the occupied probability across all nonempty classes but also leverages the entire probability distribution. Compared

Table 5: **Separate results on SemanticKITTI and KITTI360.** We evaluate our Depth-UP models on two datasets. The default evaluation range is $51.2\times51.2\times6.4\text{m}^3$. Due to the label differences between the two subsets, missing labels are replaced with "-". "Depth-UP$^*$" means the VoxFormer with our Depth-UP method. "Depth-UP$^\dagger$" means the OccFormer with our Depth-UP method. "Depth-UP$^\ddagger$" means the CGFormer with our Depth-UP method. The top three performances on each dataset are marked by **red**, **green**, and **blue** respectively.

| Dataset | Method | Input | IoU | mIoU | car | bicycle | motorcycle | truck | other-veh. | person | road | parking | sidewalk | other-grnd | building | fence | vegetation | terrain | pole | traf.-sign | bicyclist | trunk | motorcyclist |
|---|---|---|---|---|---|---|---|---|---|---|---|---|---|---|---|---|---|---|---|---|---|---|---|
| SemanticKITTI | LMSCNet | L | 38.36 | 9.94 | 23.62 | 0.00 | 0.00 | 1.69 | 0.00 | 0.00 | 54.9 | 9.89 | 25.43 | 0.00 | 14.55 | 3.27 | 20.19 | 32.30 | 2.04 | 0.00 | 0.00 | 1.06 | 0.00 |
| | SSCNet | L | 40.93 | 10.27 | 22.32 | 0.00 | 0.00 | 4.69 | 2.43 | 0.00 | 51.28 | 9.07 | 22.38 | 0.02 | 15.2 | 3.57 | 22.24 | 31.21 | 4.83 | 1.49 | 0.01 | 4.33 | 0.00 |
| | MonoScene | C | 36.80 | 11.30 | 23.29 | 0.28 | 0.59 | 9.29 | 2.63 | 2.00 | 55.89 | 14.75 | 26.50 | 1.63 | 13.55 | 6.60 | 17.98 | 29.84 | 3.91 | 2.43 | 1.07 | 2.44 | 0.00 |
| | VoxFormer | C | 44.02 | 12.35 | 25.79 | 0.59 | 0.51 | 5.63 | 3.77 | 1.78 | 54.76 | 15.50 | 26.35 | 0.70 | 17.65 | 7.64 | 24.39 | 29.96 | 7.11 | 4.18 | 3.32 | 5.08 | 0.00 |
| | TPVFormer | C | 35.61 | 11.36 | 23.81 | 0.36 | 0.05 | 8.08 | 4.35 | 0.51 | 56.50 | 20.60 | 25.87 | 0.85 | 13.88 | 5.94 | 16.92 | 30.38 | 3.14 | 1.52 | 0.89 | 2.26 | 0.00 |
| | OccFormer | C | 36.50 | 13.46 | 25.09 | 0.81 | 1.19 | 25.53 | 8.52 | 2.78 | 58.85 | 19.61 | 26.88 | 0.31 | 14.40 | 5.61 | 19.63 | 32.62 | 4.26 | 2.86 | 2.82 | 3.93 | 0.00 |
| | CGFormer | C | 44.92 | 15.82 | 34.07 | 2.87 | 4.26 | 5.80 | 6.63 | 1.51 | 66.46 | 21.27 | 33.06 | 0.00 | 21.77 | 9.18 | 25.87 | 40.18 | 10.73 | 7.02 | 3.13 | 8.62 | 0.00 |
| | Depth-UP$^*$ (ours) | C | 45.85 | 13.36 | 28.51 | 0.12 | 3.57 | 12.01 | 4.23 | 2.24 | 55.72 | 14.38 | 26.20 | 0.10 | 20.58 | 7.70 | 26.24 | 30.26 | 8.03 | 5.81 | 1.18 | 7.03 | 0.00 |
| | Depth-UP$^\dagger$ (ours) | C | 41.97 | 14.56 | 26.53 | 1.12 | 1.54 | 10.64 | 9.37 | 2.63 | 62.38 | 21.58 | 29.79 | 1.97 | 18.85 | 7.69 | 24.68 | 34.09 | 7.86 | 5.82 | 1.61 | 7.40 | 0.00 |
| | Depth-UP$^\ddagger$ (ours) | C | 48.64 | 17.02 | 34.84 | 2.43 | 6.40 | 5.26 | 10.07 | 2.26 | 66.47 | 20.47 | 33.12 | 0.26 | 27.36 | 10.11 | 29.82 | 42.72 | 12.12 | 7.71 | 2.86 | 8.52 | 0.00 |
| KITTI-360 | LMSCNet | L | 47.53 | 13.65 | 20.91 | 0 | 0 | 0.26 | 0 | 0 | 62.95 | 13.51 | 33.51 | 0.2 | 43.67 | 0.33 | 40.01 | 26.80 | 0 | 0 | - | - | - |
| | SSCNet | L | 53.58 | 16.95 | 31.95 | 0 | 0.17 | 10.29 | 0.58 | 0.07 | 65.7 | 17.33 | 41.24 | 3.22 | 44.41 | 6.77 | 43.72 | 28.87 | 0.78 | 0.75 | - | - | - |
| | MonoScene | C | 37.87 | 12.31 | 19.34 | 0.43 | 0.58 | 8.02 | 2.03 | 0.86 | 48.35 | 11.38 | 28.13 | 3.22 | 32.89 | 3.53 | 26.15 | 16.75 | 6.92 | 5.67 | - | - | - |
| | VoxFormer | C | 38.76 | 11.91 | 17.84 | 1.16 | 0.89 | 4.56 | 2.06 | 1.63 | 47.01 | 9.67 | 27.21 | 2.89 | 31.18 | 4.97 | 28.99 | 14.69 | 6.51 | 6.92 | - | - | - |
| | Depth-UP$^*$ (ours) | C | 43.25 | 13.55 | 22.32 | 1.96 | 1.58 | 9.43 | 2.27 | 3.13 | 53.50 | 11.86 | 31.63 | 3.20 | 34.49 | 6.11 | 32.01 | 18.78 | 11.46 | 13.65 | - | - | - |

Table 6: For the KITTI360 and VoxFormer, compare our HCP (referred to as "Ours") with standard conformal prediction (SCP) and class-conditional conformal prediction (CCCP) on CovGap and AvgSize. "Ours*" are results of our HCP + Depth-UP under the same defined error rate for the base model.

| Method | Base | | | | Our Depth-UP | | |
|---|---|---|---|---|---|---|---|
| CP | SCP | CCCP | Ours | Ours* | SCP | CCCP | Ours |
| CovGap ↓ | 0.64 | 0.26 | 0.10 | 0.08 | 0.62 | 0.25 | 0.10 |
| AvgSize ↓ | 6.30 | 1.03 | 0.56 | 0.49 | 13.24 | 1.51 | 1.12 |

with the class score, which only considers individual class probabilities, our score function accounts for all nonempty classes. Predicting rare classes is challenging for models, but they tend to identify these as occupied, assigning lower probabilities to the empty class and higher probabilities to all nonempty classes. Therefore, it's crucial to consider the probability of all nonempty classes. Although the occupied score addresses this by summing probabilities of all nonempty classes, it loses sensitivity to the distribution. When facing difficult samples (such as rare classes), models tend to produce output probabilities that are more evenly distributed across the possible classes (Guo et al. (2017)). The Kullback-Leibler (KL) divergence measures how one probability distribution diverges from a reference distribution, considering the entire shape of the probability distribution (Raiber & Kurland (2017)). This sensitivity to distribution shape enables our KL-based score function to identify rare classes more effectively.

**Ablation Study.** We compare our HCP with SCP and CCCP under different desired class-specific error rate settings on more OCC models: the basic OccFormer, the OccFormer with our Depth-UP, the basic CGFormer, the CGFormer with our Depth-UP, and the LiDAR-based OCC model LMSCNet (Roldao et al. (2020)) to show the scalability of our HCP. The dataset used here is SemanticKITTI. For each class, the desired error rate is set by multiplying the original error rate of OCC models with the scale $\lambda$, $\lambda \in \{0.86, 0.89, 0.92, 0.95, 0.98\}$, which raises the coverage requirement. Figure 8 shows the CovGap vs, AvgSize results. We can see that our HCP always outperforms the two baselines for the points of our HCP are located in the left bottom corner, compared with points of SCP and CCCP. Figure 9 shows the detailed results of CovGap vs. scale and AvgSize vs. scale. For most cases, as the desired error rate becomes smaller, the set size tends to be larger in order to satisfy the coverage guarantee. The results on the LiDAR-based OCC model LMSCNet (Roldao

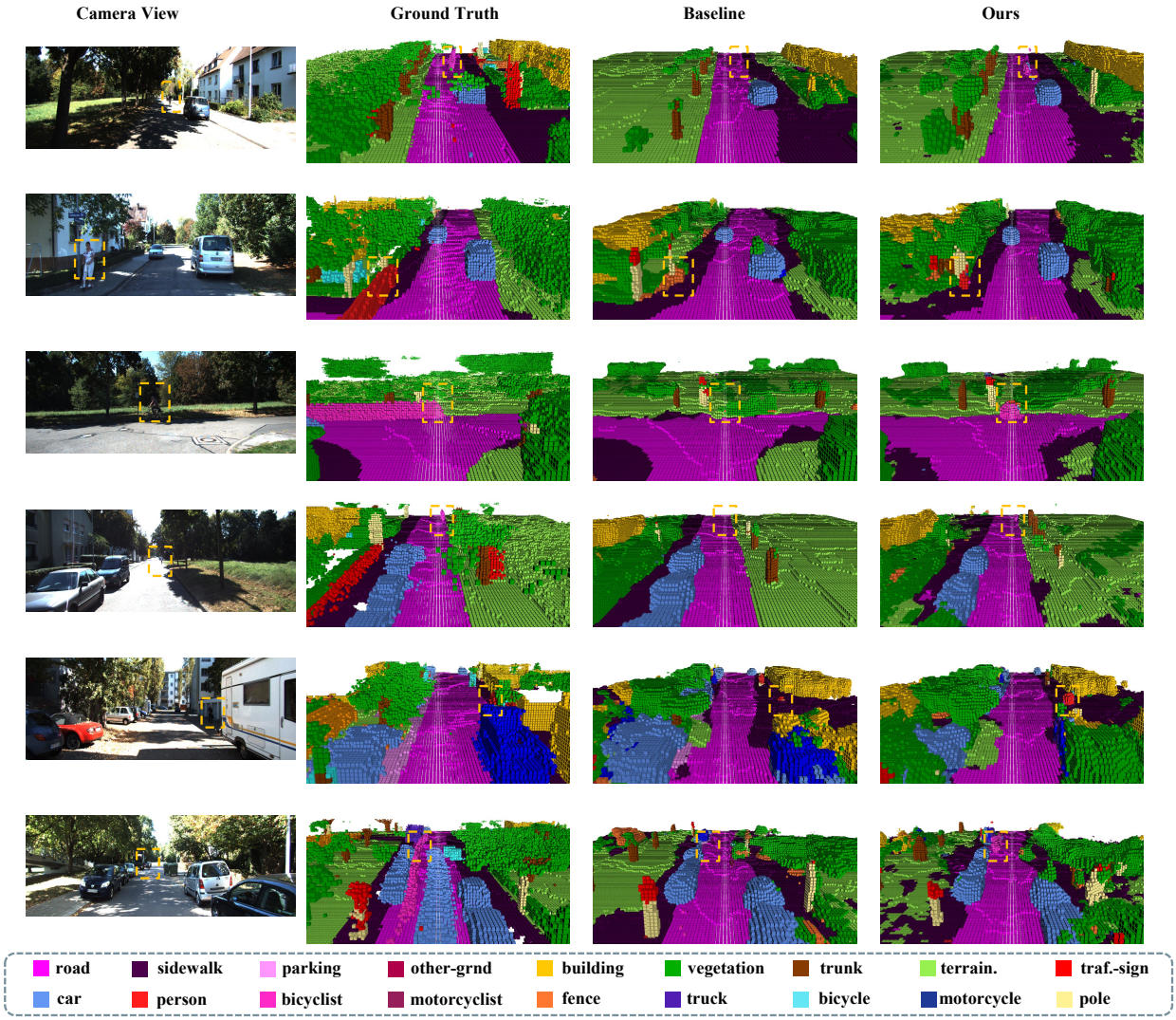


Figure 7: Qualitative results of the baseline OCC model and that with our Depth-UP method.

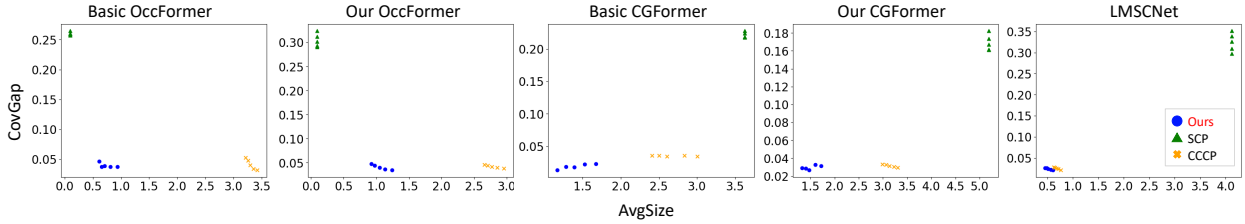


Figure 8: The results of CovGap vs, AvgSize for our HCP, SCP and CCCP on SemanticKITTI. The considered OCC models are the basic OccFormer, the OccFormer with our Depth-UP, the basic CGFormer, the CGFormer with our Depth-UP, and the LiDAR-based OCC model LMSCNet.

et al. (2020)) show that our HCP is effective in LiDAR-based OCCs, even though they are not the primary focus of our work.

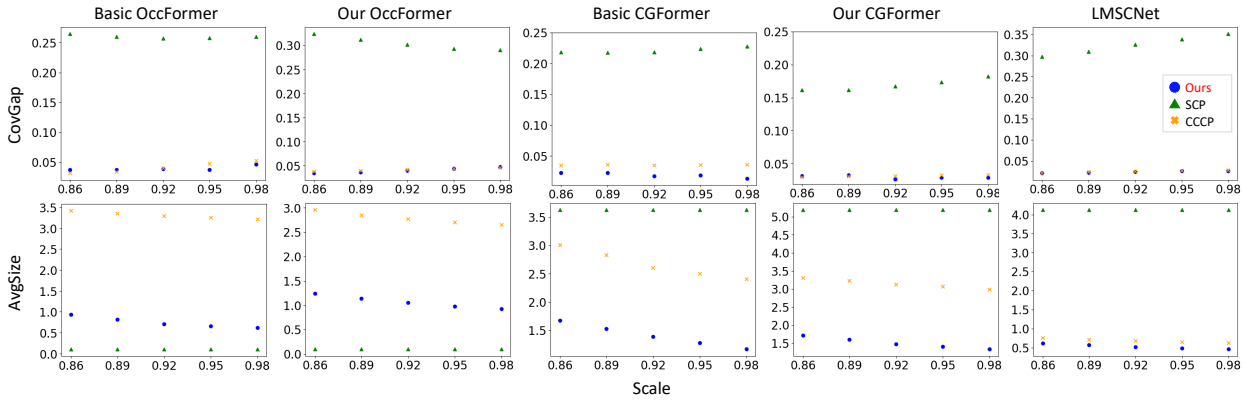


Figure 9: The results of CovGap vs. scale and AvgSize vs. scale for our HCP, SCP and CCCP on SemanticKITTI. The considered OCC models are the basic OccFormer, the OccFormer with our Depth-UP, the basic CGFormer, the CGFormer with our Depth-UP, and the LiDAR-based OCC model LMSCNet. The scale represents the desired class error rate.

### A.9 Experimental Results on Occ3D-nuScenes Dataset

To demonstrate the scalability of our $\alpha$-OCC approach, we applied it to the Occ3D-nuScenes dataset (Caesar et al. (2020)) and the OCC model BEVStereo (Li et al. (2023c)).

The Occ3D-nuScenes dataset consists of 1,000 outdoor driving scenes captured using six surround-view cameras. The sparse input to the OCC model comprises six RGB images from these cameras. The dataset features voxel grids labeled with 17 classes (16 semantic classes and 1 empty class) at a resolution of 0.4m $\times$ 0.4m $\times$ 0.4m. We utilized only the training and validation sets of NuScenes, as the test set annotations are unavailable. The 3D volume of interest covers a range of 40m ahead and behind the vehicle, 40m to the left and right sides, 1m below, and 5.4m above the vehicle. BEVStereo (Li et al. (2023c)) serves as a commonly used OCC baseline for the Occ3D-nuScenes dataset in many works, such as RenderOcc (Pan et al. (2024)) and PanoOcc (Wang et al. (2024)). Due to time and computational constraints, both the base BEVStereo model and BEVStereo with our Depth-UP were trained for 12 epochs and 20 batch sizes on the server with 4 Tesla V100 GPUs while the original work trained on 32 batch sizes. The input image size here is 416 $\times$ 704 while the original work used the 512 $\times$ 1408 input image size.

Table 7 presents the mIoU across all classes and the IoU for each individual class for both the base BEVStereo model and BEVStereo enhanced with our Depth-UP on the Occ3D-nuScenes dataset. Depth-UP demonstrates notable improvements over the base OCC model, achieving a 1.61 (8.77%) increase in mIoU. Furthermore, our Depth-UP significantly enhances performance for small, safety-critical classes, including a 9.43 IoU improvement for the motorcycle class and a 1.09 IoU improvement for the person class. These improvements are attributed to the effective integration of uncertainty information from the depth model into the OCC model.

Table 8 compares our HCP method with SCP and CCCP on the Occ3D-nuScenes dataset using the BEVStereo model, similar to Table 2. The results demonstrate that HCP consistently achieves robust empirical class-conditional coverage while generating smaller prediction sets. Compared to SCP, it reduces the set size by up to 87% and the coverage gap by up to 97%. Similarly, compared to CCCP, it achieves reductions of up to 10% set size and 6% coverage gap. These findings are consistent with experimental results on the SemanticKITTI and KITTI360 datasets, further validating the scalability of our approach.

### A.10 Ablation Study on Model Parameter

Due to space limitations, we did not include the changes in model parameters for our Depth-UP approach in Table 3. Here, we provide a discussion. The original model size is 59.98MB. Adding a head for depth uncertainty estimation increases the size to 60.09MB, representing a 0.18% increase. The Propagation on

Table 7: Separate results of our Depth-UP on the Occ3D-nuScenes dataset (Caesar et al. (2020)) and the BEVStereo (Li et al. (2023c)) model.

| Method | mIoU | motorcycle | person | traffic-cone | drive.-surf. | other-flat | sidewalk | terrain | vegetation | manmade | barries | bicycle | bus | car | const.-veh. | trailer | truck | others |
|---|---|---|---|---|---|---|---|---|---|---|---|---|---|---|---|---|---|---|
| Base | 18.35 | 0.00 | 6.57 | 0.00 | 50.85 | 24.54 | 28.89 | 21.56 | 16.14 | 16.09 | 29.54 | 0.00 | 33.58 | 36.62 | 10.60 | 11.23 | 25.81 | 0.01 |
| Our | 19.96 | 9.43 | 7.66 | 1.71 | 54.01 | 26.84 | 29.76 | 26.19 | 19.14 | 14.44 | 31.74 | 0.01 | 32.55 | 33.43 | 14.25 | 10.00 | 25.02 | 3.10 |

Table 8: Compare our HCP (referred to as "Ours") with the standard conformal prediction (SCP) and class-conditional conformal prediction (CCCP) on CovGap and AvgSize for the Occ3D-nuScenes dataset and the BEVStereo model.

| Method | Base | | | Our Depth-UP | | |
|---|---|---|---|---|---|---|
| CP | SCP | CCCP | Ours | SCP | CCCP | Ours |
| CovGap ↓ | 0.1931 | 0.0070 | 0.0069 | 0.2058 | 0.0075 | 0.0070 |
| AvgSize ↓ | 0.2481 | 0.0341 | 0.0316 | 0.2585 | 0.0376 | 0.0336 |

Geometry Completion (PGC) does not introduce additional parameters beyond this head. In contrast, Propagation on Semantic Segmentation (PSS) increases the parameter size to 71.53MB, a 19.26% increase, primarily due to the additional ResNet backbone required for depth feature extraction. The whole Depth-UP approach, which includes all the above parts, increases the parameter size to 71.53MB. To address this, we plan to explore using a simpler backbone for depth feature extraction in future work to reduce the added parameters.

### A.11 Uncertainty vs. Distance

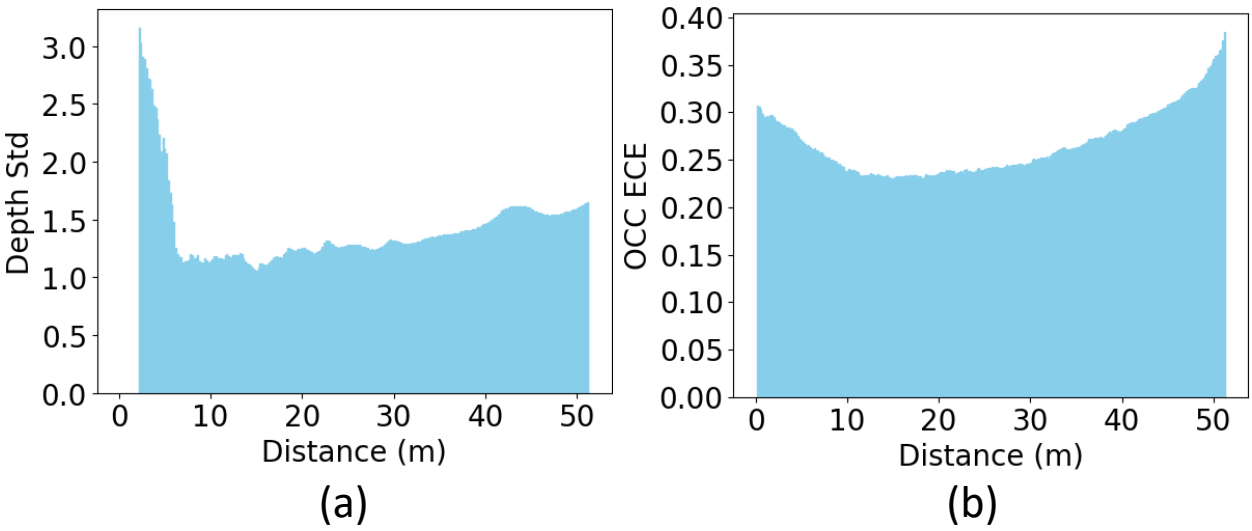


Figure 10: (a) The estimated depth standard deviation from the direct modeling method, representing uncertainty, varies with distance. (b) The Expected Calibration Error (ECE) uncertainty of the VoxFormer model output, representing OCC ECE, varies with distance.

Figure 10 illustrates the relationship between uncertainty and distance in the occupancy prediction model. In Figure 10(a), we show the correlation between the estimated standard deviation (uncertainty) of depth and the distance from the camera to the object. For clarity, we divided the distance into 256 bins, each 0.2 meters in length, and calculated the average estimated standard deviation for each bin. The results reveal that the depth uncertainty is highest when the object is very close to the camera. This phenomenon arises because, in stereo vision systems, objects at close range result in minimal disparity between the two images, making depth estimation inherently challenging (Wei et al. (2024)). The uncertainty reaches its lowest point at approximately 15 meters, beyond which it increases with distance. This trend aligns with the inverse relationship between depth and disparity, as well as the reduced pixel resolution available for objects further away from the camera (Wei et al. (2024)). These observations confirm that the depth uncertainty estimation in our model is consistent with theoretical expectations.

Figure 10(b) presents the relationship between the Expected Calibration Error (ECE) metric of the VoxFormer model and the distance to the voxels. ECE is a standard metric for assessing the calibration of uncertainty estimates in probabilistic models (Feng et al. (2021)). In this case, we applied the voxel-based ECE computation method described in Cao et al. (2024). The results show that the OCC uncertainty is minimized at approximately 15 meters, consistent with the depth uncertainty trend observed in Figure 10(a). When voxels are very close to the camera, the OCC ECE is relatively high, likely due to depth estimation errors. Similarly, when voxels are far from the camera, the OCC ECE increases, attributed to the limited pixel resolution for distant objects.

Notably, the similarity in the shapes of the curves in Figure 10(a) and 10(b) highlights the significant influence of depth uncertainty on OCC performance, as discussed in Section 1. These findings reinforce the importance of utilizing the depth uncertainty in improving final OCC performance.